

A REVIEW ON AXIAL PISTON PUMP TECHNOLOGIES

Noah D. Manring

**Glen A. Barton Professor for Fluid Power
Mechanical and Aerospace Engineering
University of Missouri**

AGENDA

- 1. My history of knowing Monika and Jaro**
- 2. A few of Monika's contributions to the field of axial piston pump research**
- 3. Physical limitations for the bandwidth frequency of an axial piston pump**

MY HISTORY OF KNOWING MONIKA AND JARO

Our first meeting ... 1995 – Ames Iowa




1955 - 2018



Our second meeting ... 1996 – Neumunster, Germany





US006220144B1

(12) **United States Patent** (10) Patent No.: **US 6,220,144 B1**
 Manring et al. (45) Date of Patent: **Apr. 24, 2001**

(54) **EXTENDED SLIPPER FOR HYDROSTATIC PUMP AND MOTOR ROTATING CYLINDERS** 2,220,636 11/1940 Bischof.
 2,277,496 3/1942 Mines.
 2,608,159 8/1952 Born.

(75) Inventors: **Noah Manring, Roland, IA (US); Jaroslav Ivantysyn, Schleswig-Holstein (DE)** 2,891,419 6/1959 Badalini.
 3,120,816 2/1964 Firth et al.
 3,142,262 7/1964 Firth et al.
 3,159,041 12/1964 Firth et al.
 3,424,097 1/1969 Molly.
 4,037,521 7/1977 McLeod.
 5,070,765 12/1991 Parsons.

(73) Assignee: **Sauer Inc., Ames, IA (US)**

(*) Notice: Subject to any disclaimer, the term of this patent is extended or adjusted under 35 U.S.C. 154(b) by 0 days.

(21) Appl. No.: **09/387,872** FOREIGN PATENT DOCUMENTS
 1 269 494 5/1968 (DE).

(22) Filed: **Jun. 3, 1997** Primary Examiner—F. Daniel Lopez
 (74) Attorney, Agent, or Firm—Zarley, McKee, Thomte, Voorhees & Sease

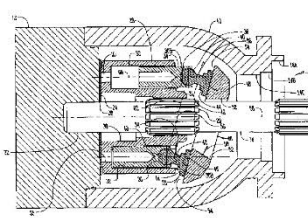
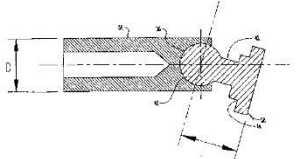
Related U.S. Application Data (57) **ABSTRACT**

(63) Continuation of application No. 08/582,656, filed on Jan. 4, 1996, now abandoned. A cylinder block for a hydrostatic transmission has a rotatable piston housing with a plurality of piston bores arranged in a circular pattern in the housing. A piston element is slidably mounted in each bore. Each of the piston elements has an outer end extendible out of an open end of each of the bores. A well or socket having a rounded bottom portion is in the outer end of each of the pistons. A piston slipper element comprising an arcuate base (a ball) is rotatably mounted in the socket. An arm extends outwardly from the ball and has a laterally extending flat planar surface at the outer end. The flat planar surface slidably engages a swashplate having a planar control surface. The distance from the center of the ball to the flat planar surface is greater than the diameter of the piston element.

(51) Int. Cl.⁷ **F01B 13/04; F01B 3/00**
 (52) U.S. Cl. **92/57; 92/71**
 (58) Field of Search 91/499; 92/12.2, 92/57, 71; 417/269; 74/60

(56) **References Cited**
 U.S. PATENT DOCUMENTS
 932,033 7/1909 Kroon.
 1,137,283 4/1915 Pratt.
 1,159,980 11/1915 Moreno.
 1,263,180 4/1918 Williams.
 1,533,399 4/1925 Dunlap.
 1,710,567 4/1929 Carey.

7 Claims, 4 Drawing Sheets

Subsequent meetings ... 2004 and beyond



**A FEW OF MONIKA'S CONTRIBUTIONS TO THE
FIELD OF AXIAL PISTON PUMP RESEARCH**



1955 - 2018

Most Recent Paper ...

Williams, K., and M. Ivantysynova. 2019. Approximate stochastic differential dynamic programming for hybrid vehicle energy management. *Journal of Dynamic Systems, Measurement and Control*. Vol. 141 051003-1-9

Approximate Stochastic Differential Dynamic Programming for Hybrid Vehicle Energy Management

Kyle Williams¹

School of Mechanical Engineering,
Purdue University,
West Lafayette, IN 47906
e-mail: kwilliams@alum1.purdue.edu

Monika Ivantysynova

Marek Fluid Power Research Center,
School of Mechanical Engineering,
Purdue University,
West Lafayette, IN 47906
e-mail: mivantys@purdue.edu

This paper develops a new computational approach for energy management in a hydraulic hybrid vehicle. The developed algorithm, called approximate stochastic differential dynamic programming (ASDDP) is a variant of the classic differential dynamic programming algorithm. The simulation results are discussed for two Environmental Protection Agency drive cycles and one real world cycle based on collected data. Flexibility of the ASDDP algorithm is demonstrated as real-time driver behavior learning, and forecasted road grade information are incorporated into the control setup. Real-time potential of ASDDP is evaluated in a hardware-in-the-loop (HIL) experimental setup.
[DOI: 10.1115/1.4042253]

1 Introduction

The hybrid vehicle offers a solution for personal, public, and commercial transportation vehicles which can significantly reduce fuel consumption and engine emissions output in comparison to conventional vehicle solutions. The stochastic nature of driver behavior and driving environment presents one of the biggest challenges in hybrid vehicle control. In both hybrid electric vehicles (HEV) and hybrid hydraulic vehicles (HHV), the controller must ensure proper charge of the energy storage system to ensure future driver demands can be satisfied while also observing system constraints and maximizing overall system efficiency. Early solutions to the hybrid vehicle control problem involved finite horizon dynamic programming (DP) simulations for predefined drive cycles. Although globally optimal, the resulting open loop control trajectories were only valid for the defined drive cycle. Heuristic feedback policies were then formulated in an attempt to replicate the properties of the open-loop control trajectories resulting from the DP simulations [1]. Other solutions have relied on model predictive control (MPC) [2], where optimization is performed along a future horizon assuming some simplified form of driver behavior. A benefit to MPC is that real-time information can be incorporated to make immediate changes to the problem formulation, resulting in a controller that is more closely tuned to present driving conditions. In Ref. [3], MPC is used for energy management of an HEV with driver torque demand modeled as an exponentially decreasing process. In Refs. [4] and [5], the horizon optimization considers forecasted information provided by on-board telematics. By incorporating a simplified model of driver behavior and information regarding the environment, MPC methods do not require the formation of policy heuristics. However, these methods ignore the underlying stochastic nature of driver behavior.

Modeling driver behavior as a Markov chain has proven an effective approach for capturing driver behavior [6–8]. Stochastic dynamic programming (SDP) [9] works directly with the Markov chain model to formulate control policies which consider possible future driver behavior, minimizing the expected cost of the objective function over a time horizon. SDP has been widely explored in the context of hybrid vehicle control [6,10–12]. Like its deterministic counterpart, SDP scales poorly to problems involving large state and action spaces. Neuro-dynamic programming (NDP) [13] alleviates the scaling issue through the use of neural

networks (NN) to represent the value function and state-feedback policy mapping. Neuro-dynamic programming is employed in Ref. [14] to minimize an impressively complex objective function comprising fuel consumption and engine emissions in an HHV. The work of Ref. [15] suggests that stochastically robust methods such as SDP may not provide optimal fuel economy when mispredictions exist. Such mispredictions can be caused, for example, when the Markov chain model used in the SDP formulation is not representative of the actual drive cycle, emphasizing the need for adaptation of the statistical model if stochastic methods are to be employed.

Stochastic model predictive control (SMPC) methods [16] combine stochastic optimization with feedback via repeated computation of an optimal predicted trajectory. A unique challenge to SMPC is the development of computationally efficient solvers which can handle the computational burden associated with stochastic optimization. A stochastic quadratic programming (QP) solver for Markov jump linear systems with transition probability estimation is presented in Ref. [17] for HEV energy management. Here, driver behavior is represented as a Markov chain and multiple scenarios are generated along a variable length horizon. To reduce computational burden, only scenarios with relatively high likelihood are considered. A method for predicting road grade is incorporated in the framework of SMPC in Ref. [18]. Here, road grade and driver behavior are modeled as independent Markov chains, and the subsequent stochastic optimization is performed with finite horizon SDP with reported execution times between 10 and 100 s on an Intel Core i7-4790 central processing unit.

Neural networks are used to predict driver acceleration demand and vehicle velocity along a finite horizon in Ref. [19]. An MPC formulation is used to carry out the finite horizon optimization. A major finding in Ref. [19] is that an MPC strategy based on NN-based velocity predictions outperforms the same strategy incorporating Markov chain-based velocity predictors. The NN and Markov chain were both trained on a large data set and evaluated on a separate data set. The authors of Ref. [19] explicitly state that no learning mechanisms were used to estimate the parameters of the Markov chain in real-time, possibly eliminating one of the most flexible and useful attributes of the Markov chain driver modeling approach for hybrid vehicle energy management.

This paper adds two original contributions to the related literature. First, a new computational method for hybrid vehicle energy management is developed. The method, called approximate stochastic differential dynamic programming (ASDDP), is a stochastic variant of differential dynamic programming [20]. ASDDP relies on the multistep Markov transition matrix to significantly reduce the computational complexity of the approach developed in Ref. [20]. A mechanism for planning beyond the finite horizon

- Hydraulic hybrid vehicles
- Energy management
- Proper charge of the energy storage system

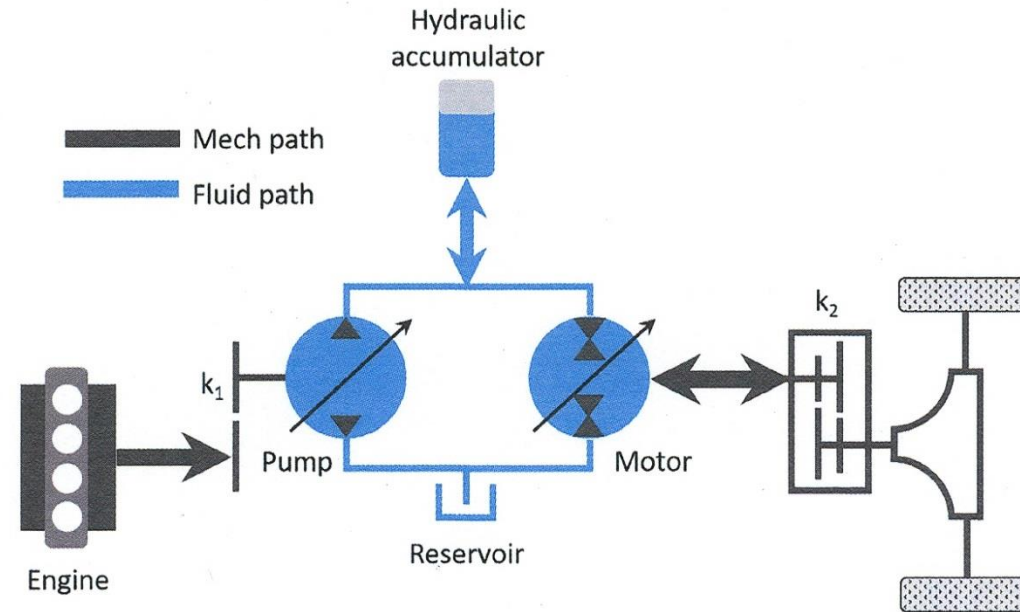


Fig. 1 Series HHV

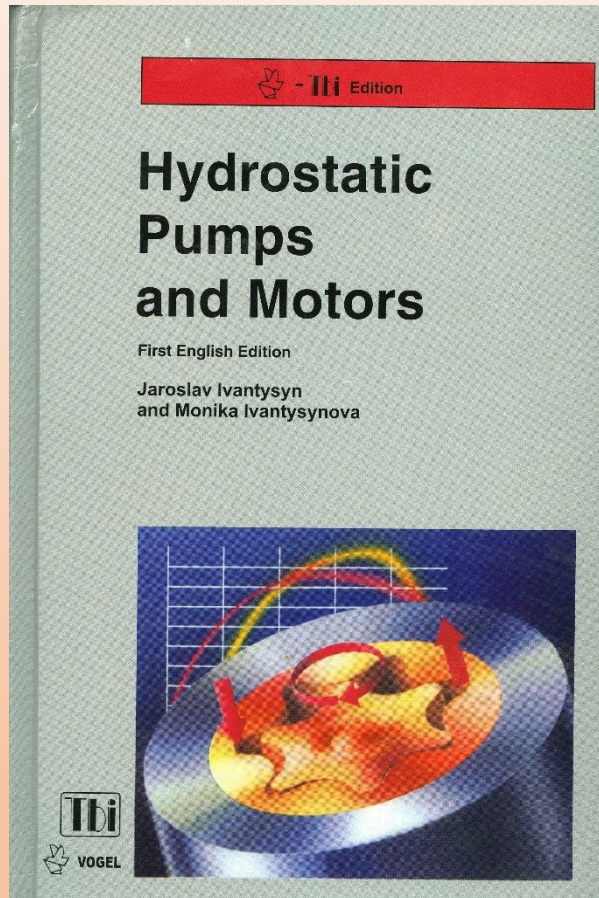
¹Present address: Caterpillar Large Power Systems Division, Lafayette, IN 47905.
Contributed by the Dynamic Systems Division of ASME for publication in the JOURNAL OF DYNAMIC SYSTEMS, MEASUREMENT, AND CONTROL. Manuscript received June 2, 2018; final manuscript received December 11, 2018; published online January 14, 2019. Assoc. Editor: Mahdi Shahbakhti.



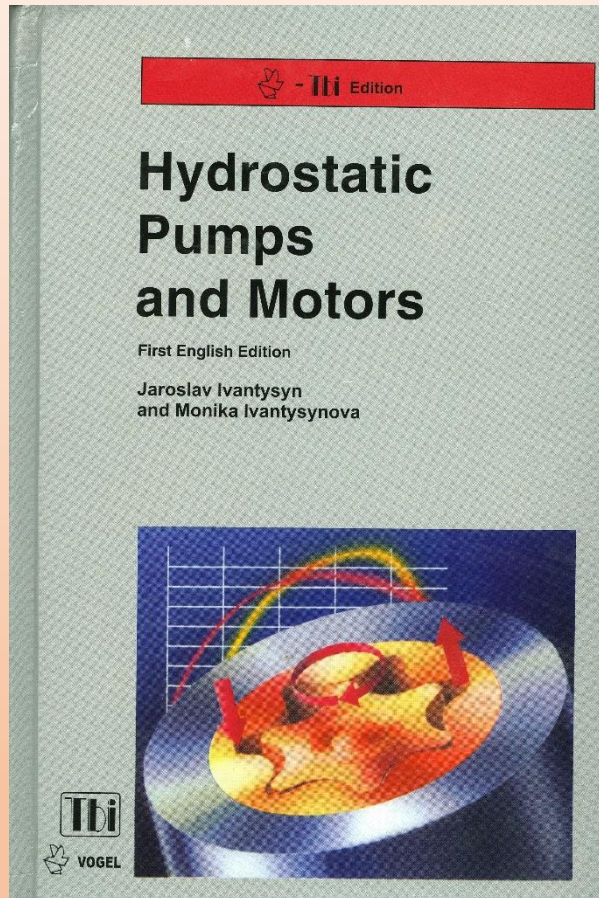
1955 - 2018

Seminal Book ...

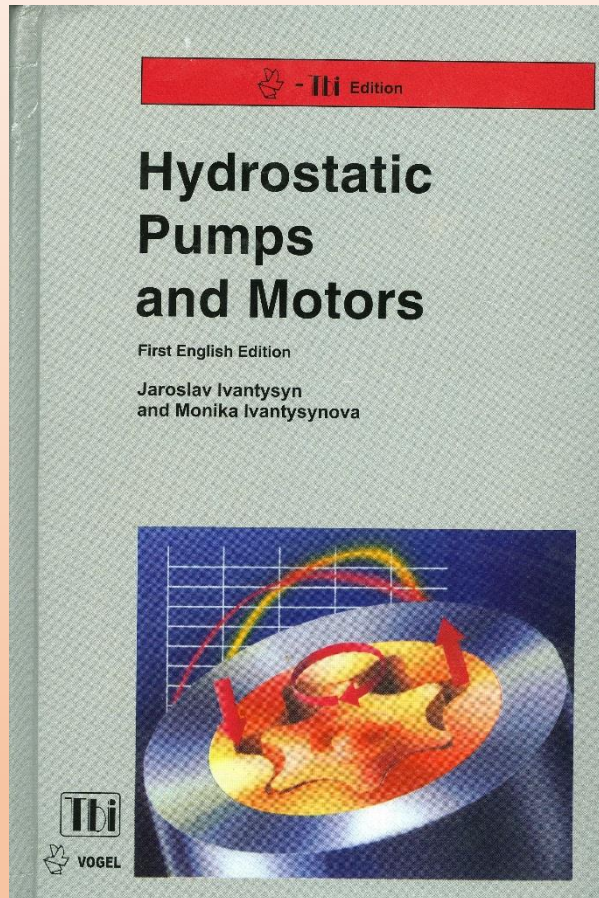
Ivantysyn, J, and M. Ivantysynova. 2003. Hydrostatic Pump and Motors: Principles, Design, Performance, Modelling, Analysis, Control and Testing. First English Edition. (First published in German, 1993.) Tech Books International. New Delhi, India.



“The main objective of this book is to provide a comprehensive account for design and analysis of hydrostatic pumps and motors similar to the popular technical literature in the classical branches of mechanical engineering like turbines, centrifugal pumps, compressors and internal combustion engines.”



“The aim of this book is not only to give the reader the possibility to understand the working principles of hydrostatic pumps and motors but he should also be able to use modern computational methods for the design and analysis of displacement machines as well as fluid power systems.”



1. Piston pumps
2. Gear pumps
3. Screw pumps
4. Vane pumps
5. Efficiency
6. Control

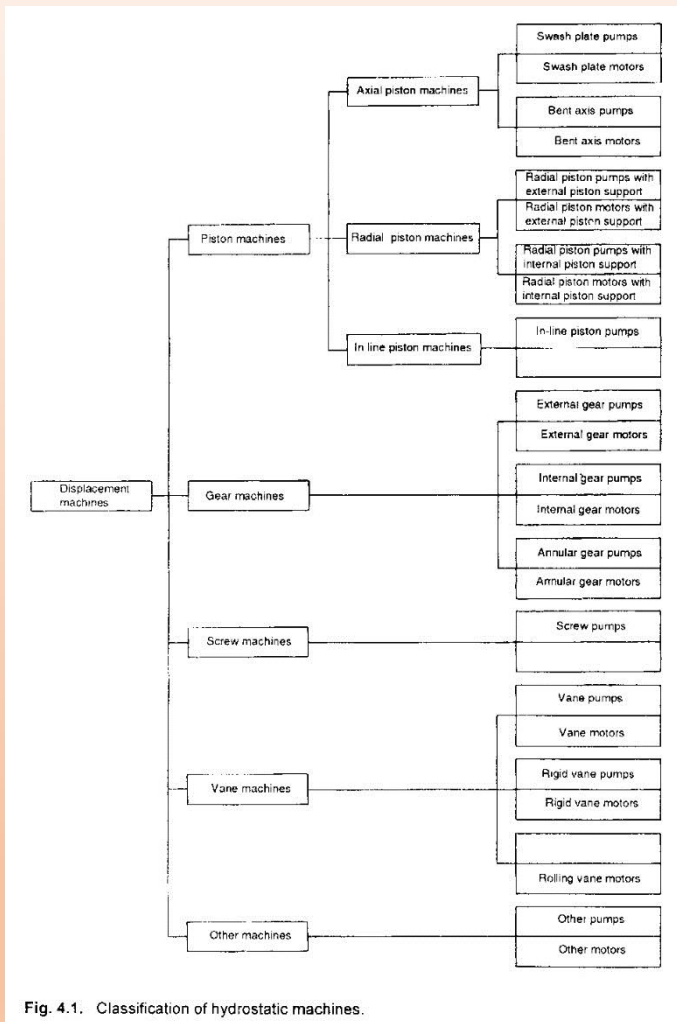


Fig. 4.1. Classification of hydrostatic machines.

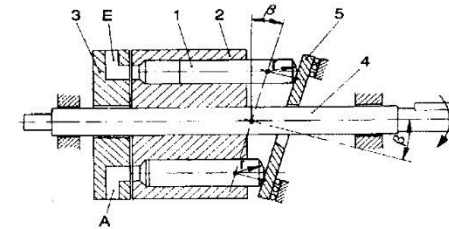


Fig. 4.9. Axial piston pump of swash-plate design with spherical cap piston (1) Piston (2) Cylinder-block (3) Valve plate (4) Drive shaft (5) Swash-plate. E inlet, A outlet.

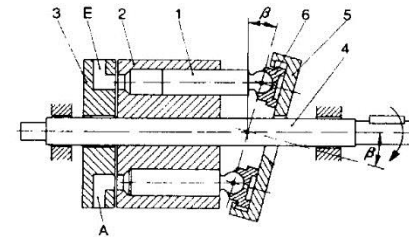


Fig. 4.10. Axial piston pump of swash plate design with slippers (1) Piston (2) Cylinder-block (3) Valve plate (4) Drive shaft (5) Swash plate (6) Slippers. E inlet, A outlet.

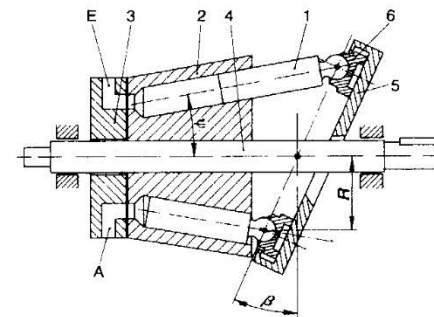


Fig. 4.11. Axial piston pump of swash-plate design with pistons arranged inclined to the shaft axis (1) Piston (2) Cylinder block (3) Valve plate (4) Drive shaft (5) Swash plate (6) Slipper. E inlet, A outlet.

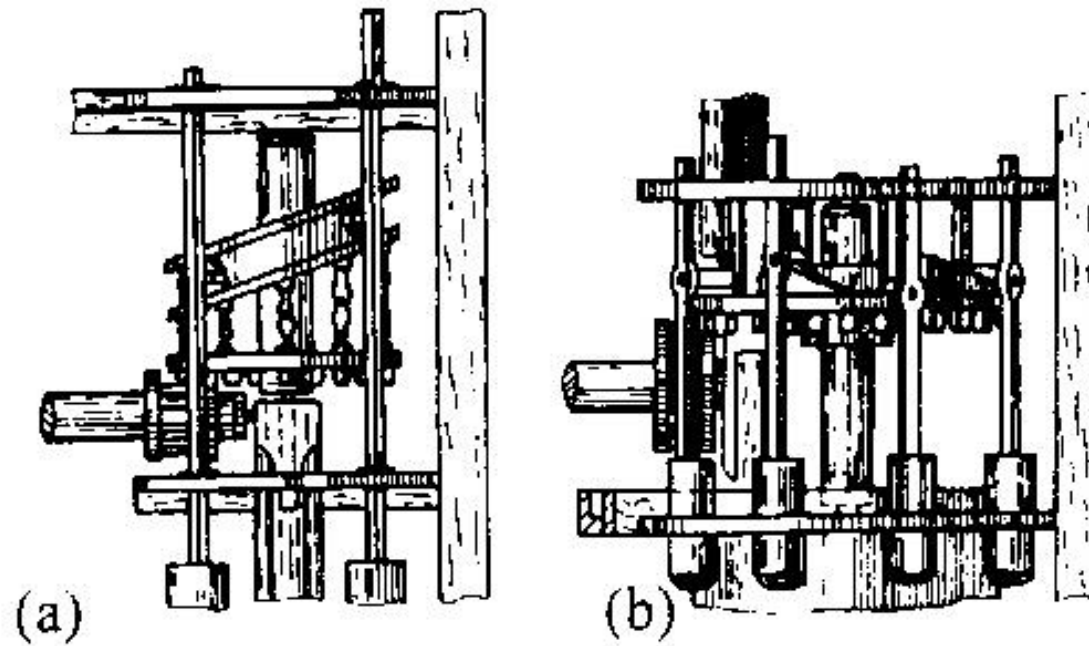
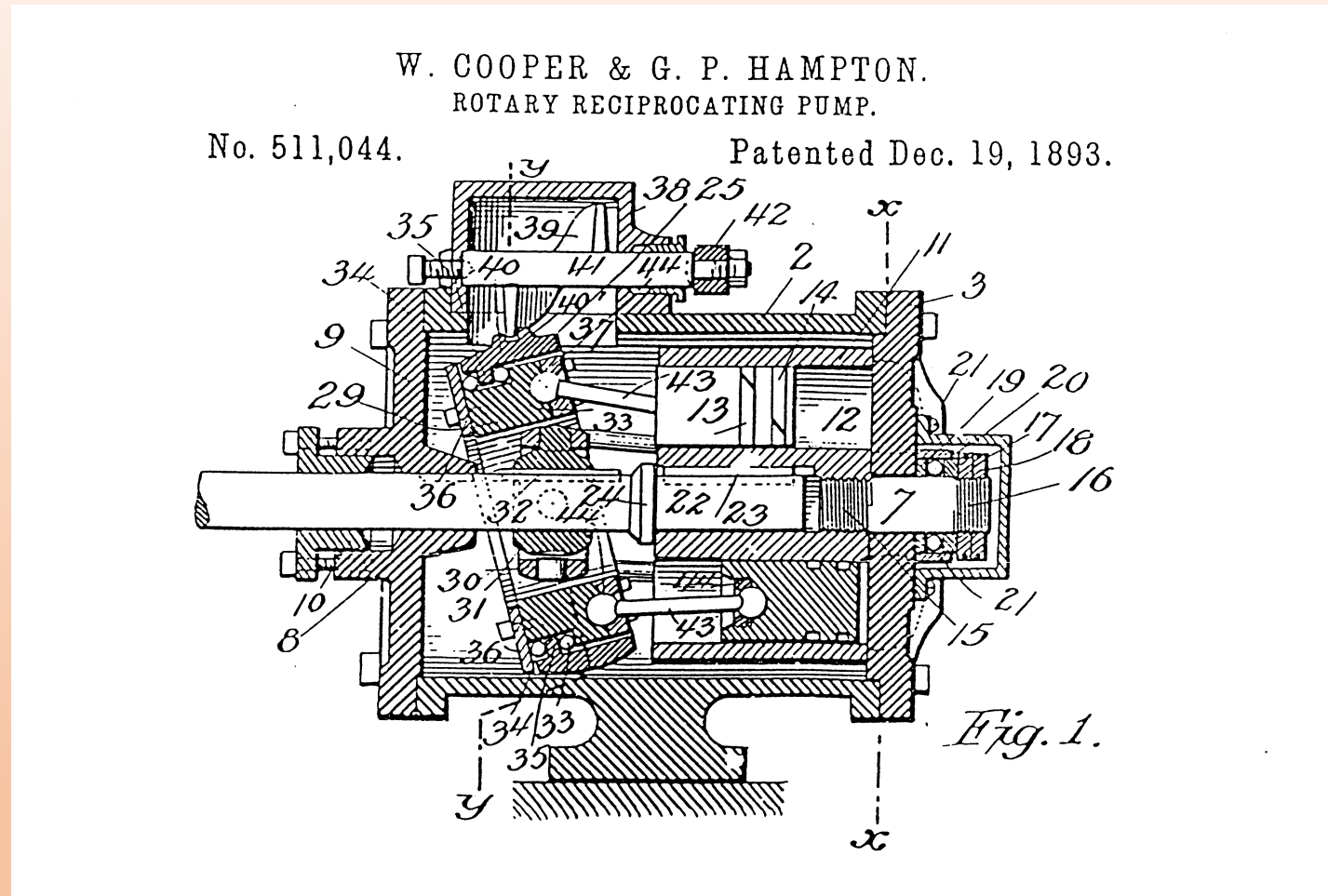


Fig. 1.6. (a) Axial piston of Ramelli in around 1600 : single stroke
(b) Axial piston pump of Ramelli developed in around 1600 : multi stroke



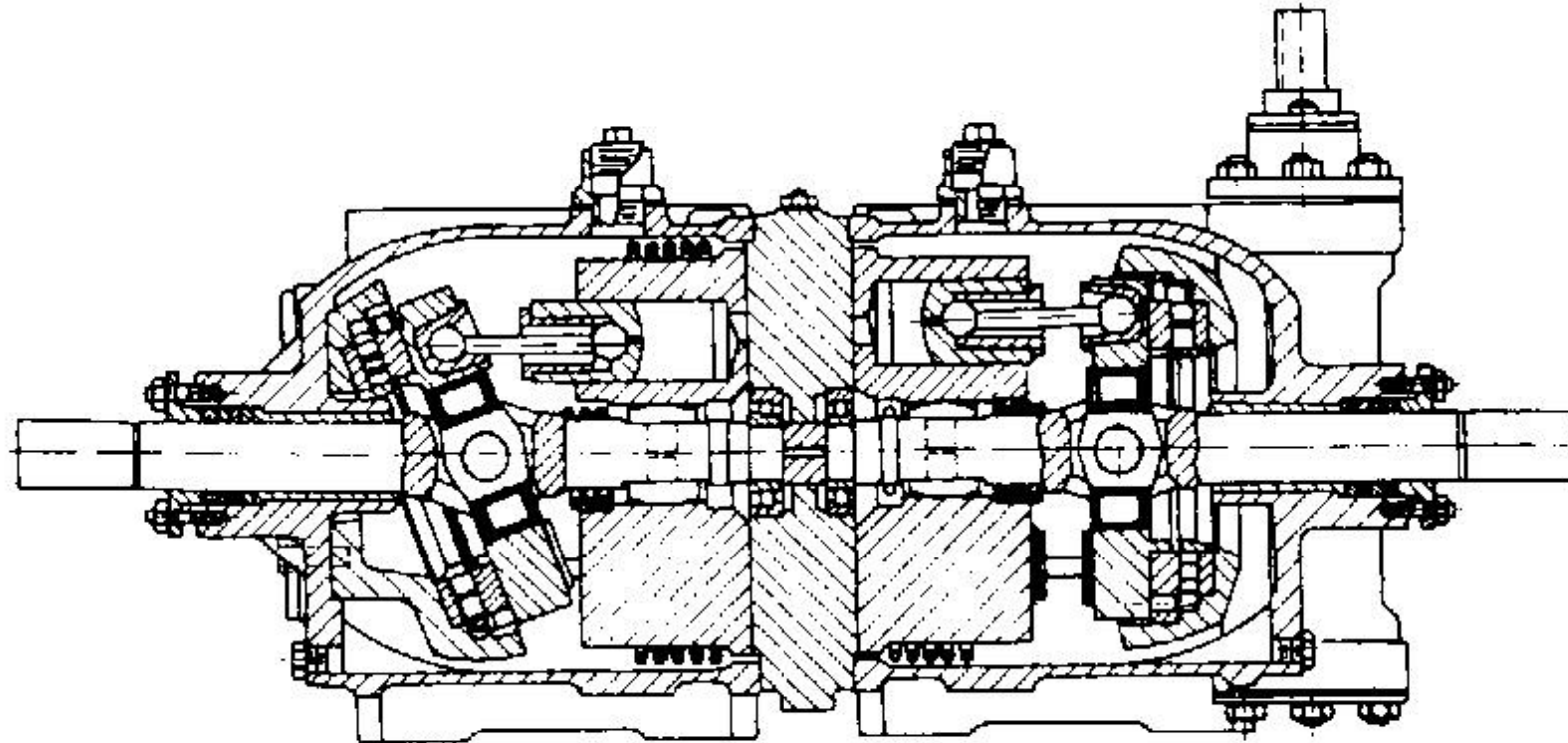


Fig. 1.8. Hydrostatic drive developed by William and Janney in 1905



1955 - 2018

Most Cited Paper ...

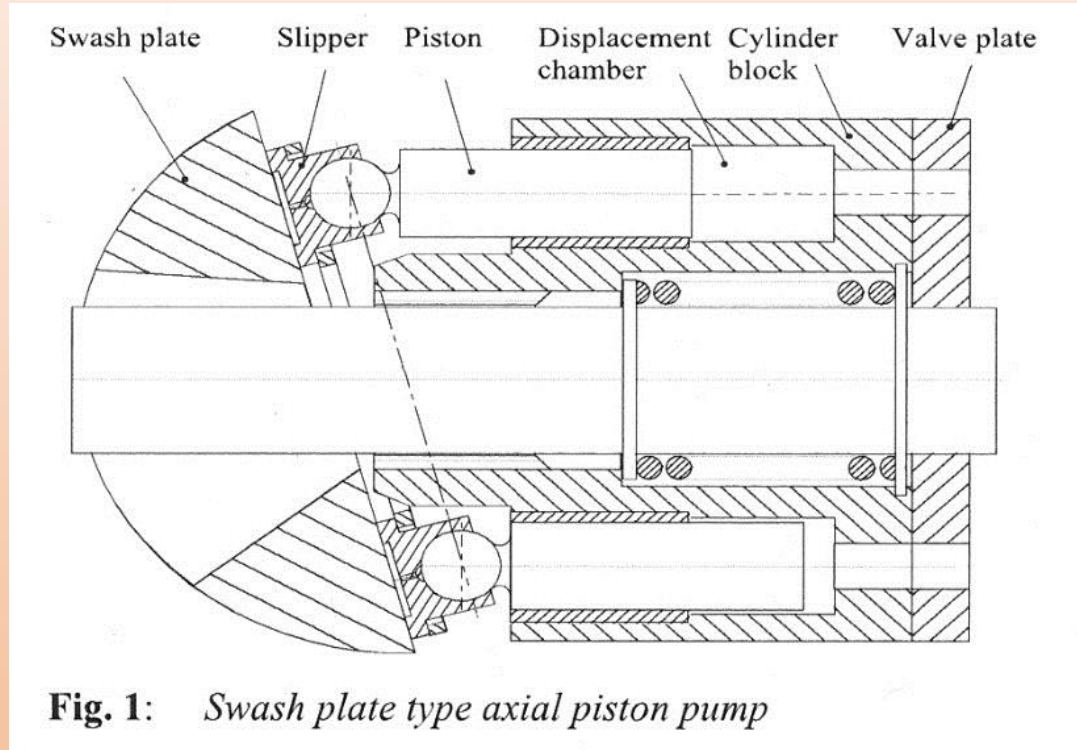
Wieczorek, U., and M. Ivantysynova. 2002. Computer aided optimization of bearing and sealing gaps in hydrostatic machines – The simulation tool CASPAR. *International Journal of Fluid Power*. Vol. 3, No. 1, pp. 7-20



- CASPAR
- **(Calculation of Swash Plate Type Axial Piston Pump and MotoR)**
- “For the first time it is possible to calculate the gap flow and thus the losses due to viscous friction and leakage in all gaps of the rotating group of a swash plate machine with the here presented simulation tool CASPAR.”
- Iterates until it finds the piston eccentricity, etc.
- Highest leakage on the low pressure side of the pump
- Accounts for local viscosity changes (leakage and friction)
- Correlates well with experimental results



1. Introduction
2. Simulation tool
3. Calculation of gap flow
4. Pressure in the displacement chamber
5. Motion equation
6. Simulation results
 - a. Piston
 - b. Slipper
 - c. Cylinder block
 - d. Total losses
 - e. Swash plate moment
7. Conclusion



Introduction ...

- Conducted at the Technical University of Hamburg-Harburg (2nd stint, 1999-2004)
- Volumetric and friction losses
- Numerical solutions for PDEs (Reynolds equation and Energy equation)
- “For the first time it is possible to calculate the gap flow and thus the losses due to viscous friction and leakage in all gaps of the rotating group of a swash plate machine with the here presented simulation tool CASPAR.”

Simulation tool ...

- Numerical solutions for PDEs (Reynolds equation and Energy equation)
- Iteration is done to solve the motion equation (eccentricity for pistons)
- MATLAB programing plus the graphical user interface

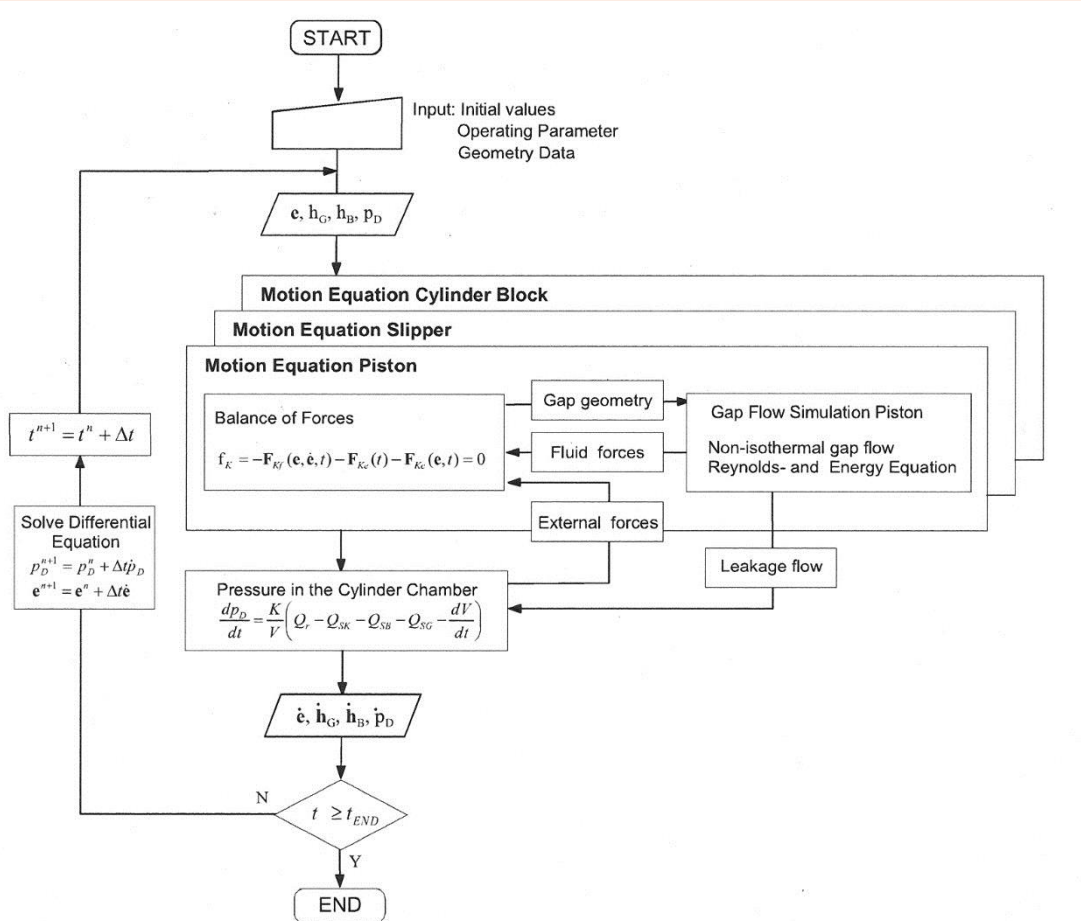
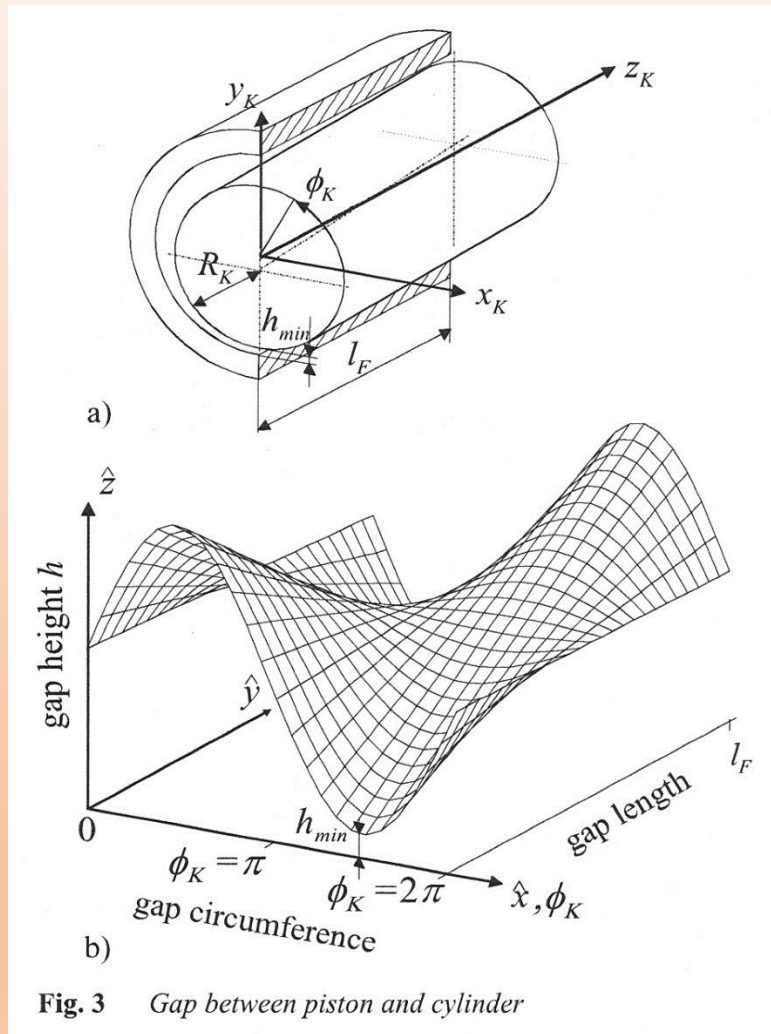


Fig. 2: Structure of the Simulation Tool CASPAR



Calculation of gap flow ...

- Laminar flow is assumed (low Reynolds number)
- 2 dimensional Reynolds equation is solved numerically
- Negative pressures are set to zero
- Local changes in viscosity are calculated using a model that adjusts for local pressure and temperature
- Energy equation is solved numerically to calculate the local temperatures
- Incompressible fluid
- Finite volume method is used to solve the PDEs (Pantankar 1980)

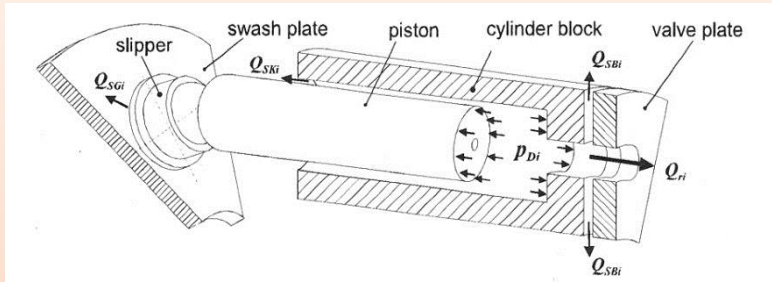


Fig. 5: Displacement chamber

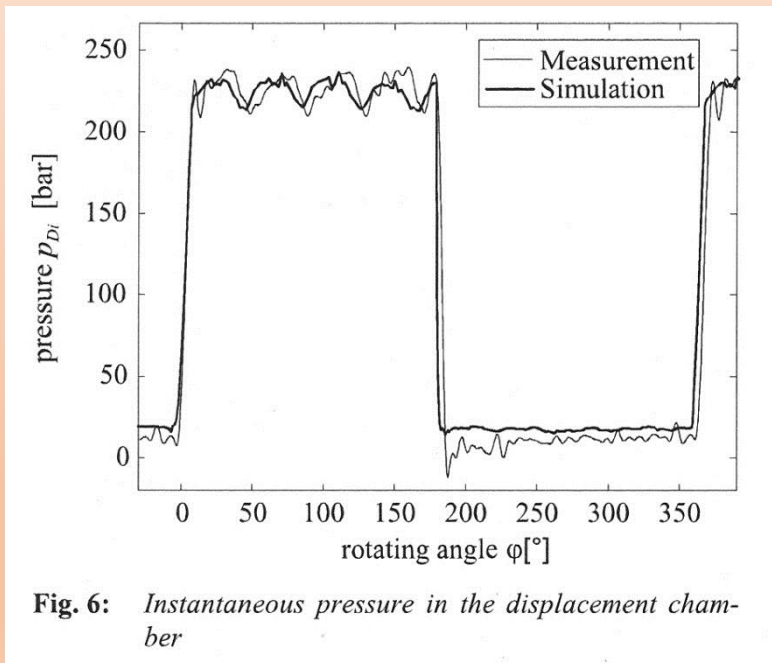


Fig. 6: Instantaneous pressure in the displacement chamber

Pressure in the displacement chamber ...

- Pressure-rise-rate equation with fluid compressibility
- Leakage calculations (3 places) coupled to the PDE solution for gap flow
- Simple model for valve-plate flow
- 75cc test machine
- Correlates well with experiments

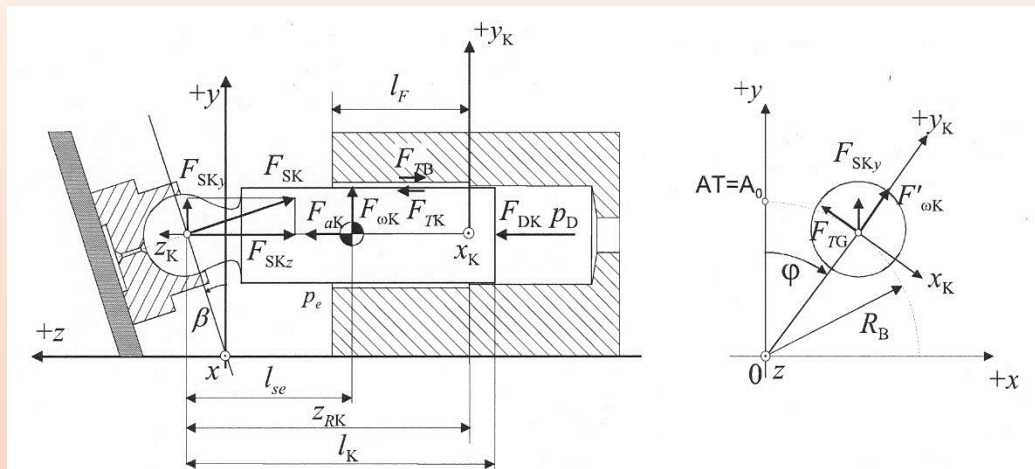
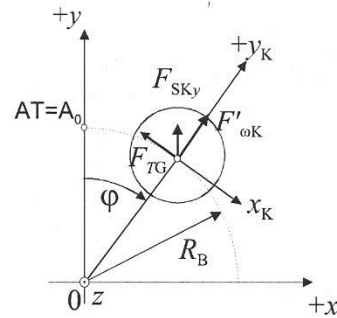


Fig. 7: External forces applied on the piston



Motion equation ...

- Static equation of forces acting on the piston (inertia is neglected)
- Squeeze film equations are used to create an ODE for modeling the motion of the piston in the radial direction
- Eccentricity in 2 places, in 2 directions is calculated
- If metal-to-metal contact is found, the piston is assumed to deform elastically
- Effects of hydrodynamic lubrication were not considered at this stage ...

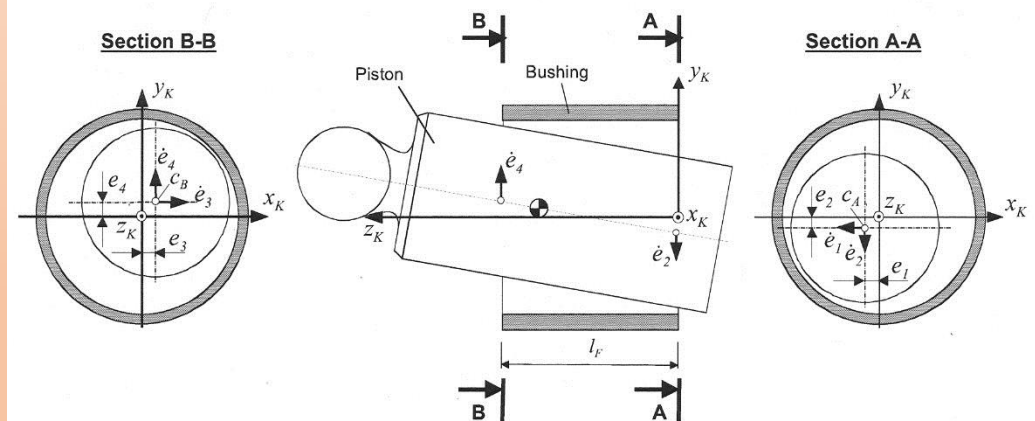


Fig. 8: Radial movement of the piston

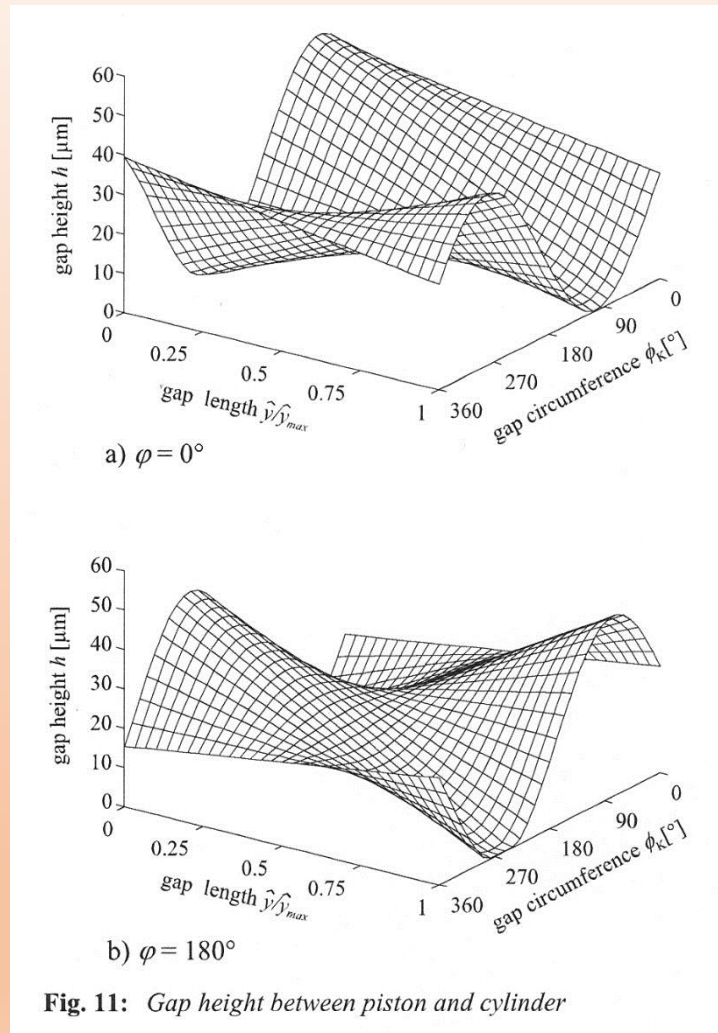


Fig. 11: Gap height between piston and cylinder

Simulation results – piston ...

- Gap height is calculated as shown in the figure
- “During the high-pressure phase the leakage flow is less than during the low-pressure phase. This can be explained by the fact that Couette flow has a stronger influence than Poiseuille flow.”
- Piston friction forces (not shown here) are comparable to measurements taken on a special test rig.

Simulation results – slipper ...

- Leakage flow during low pressure is larger than the leakage during high pressure

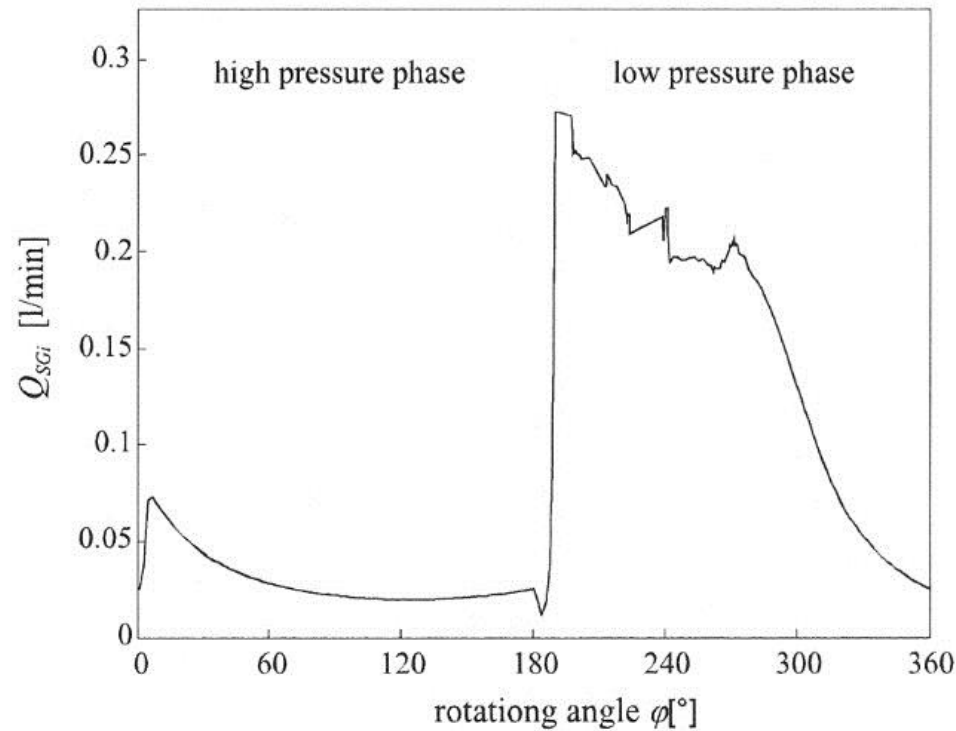


Fig. 18: Gap flow between one slipper and the swash plate

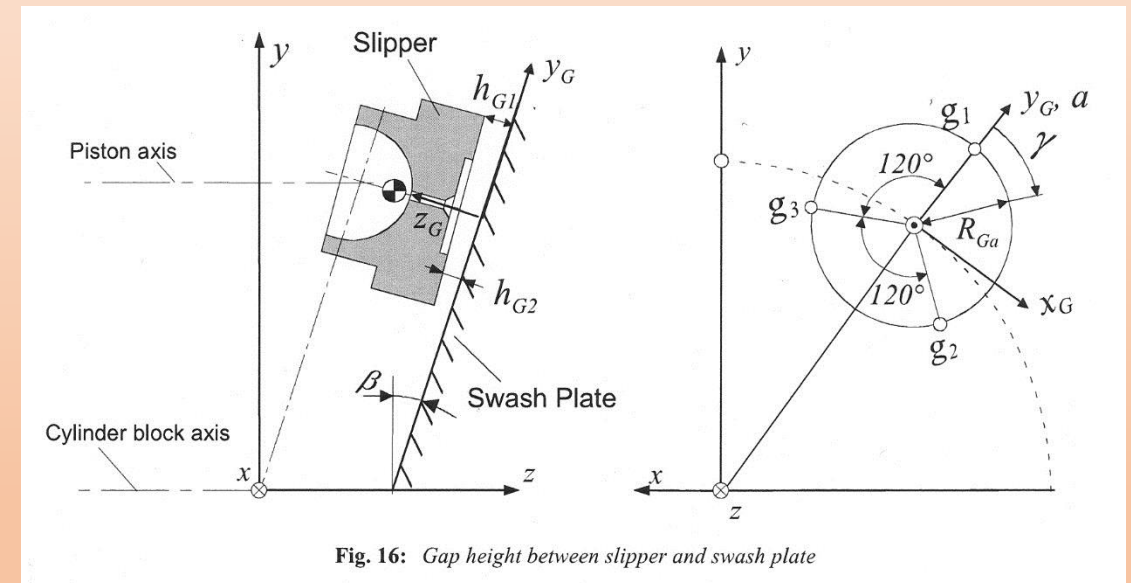
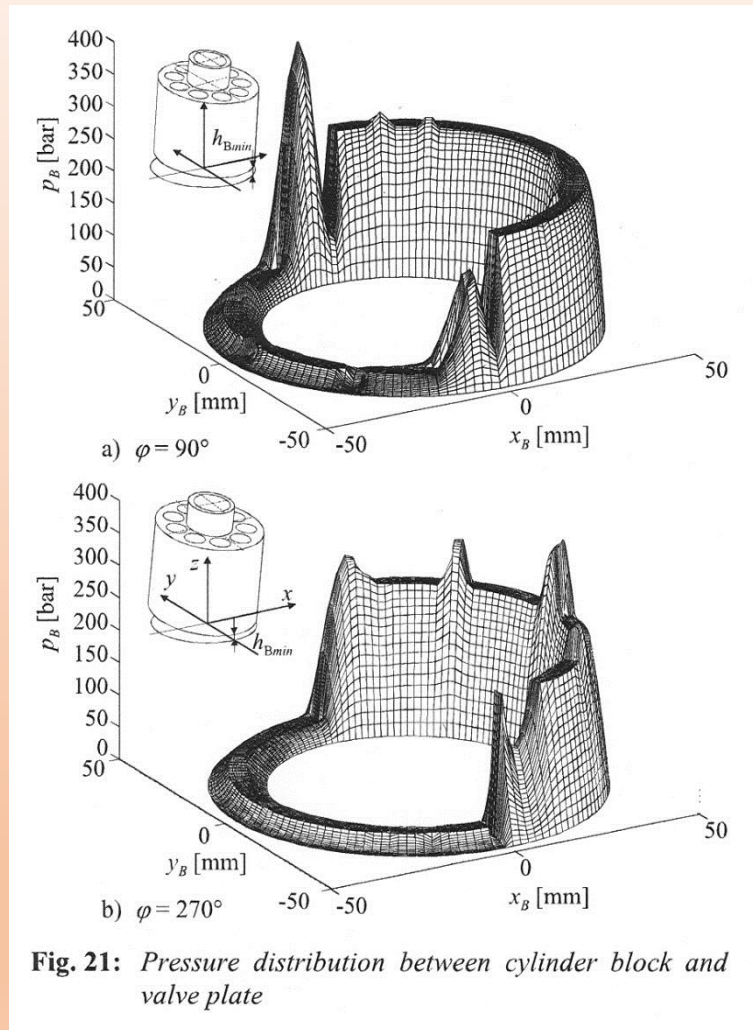
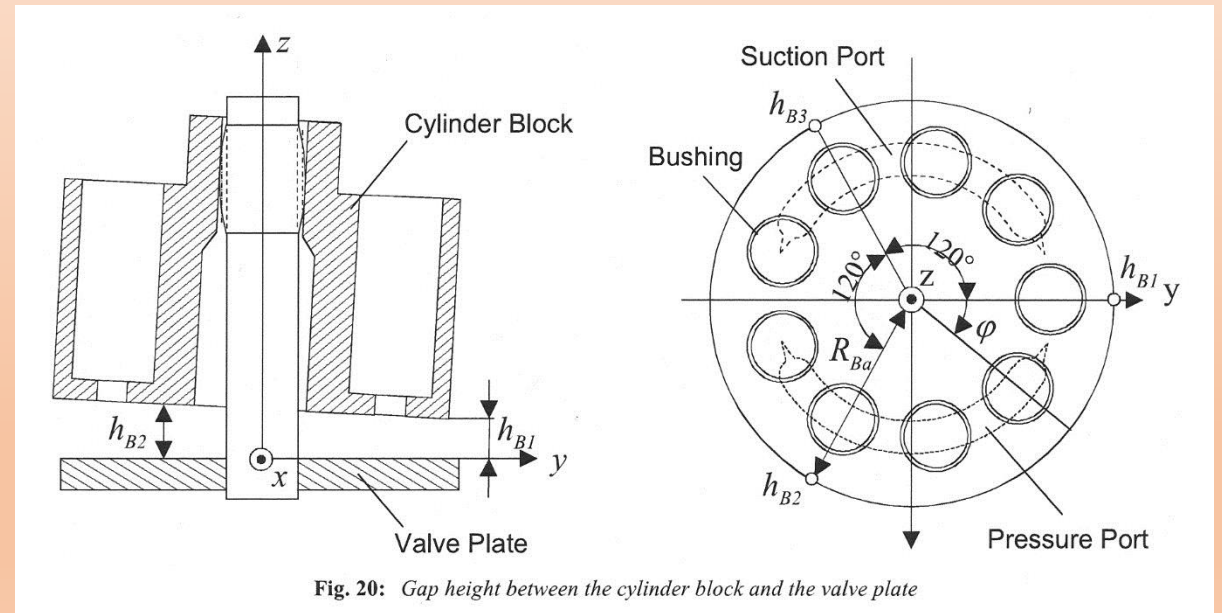


Fig. 16: Gap height between slipper and swash plate



Simulation results – cylinder block ...

- Tilting moment resisted by the valve plate
- Fluid film thicknesses ~ 2 microns
- Torque loss ~ 22 Nm



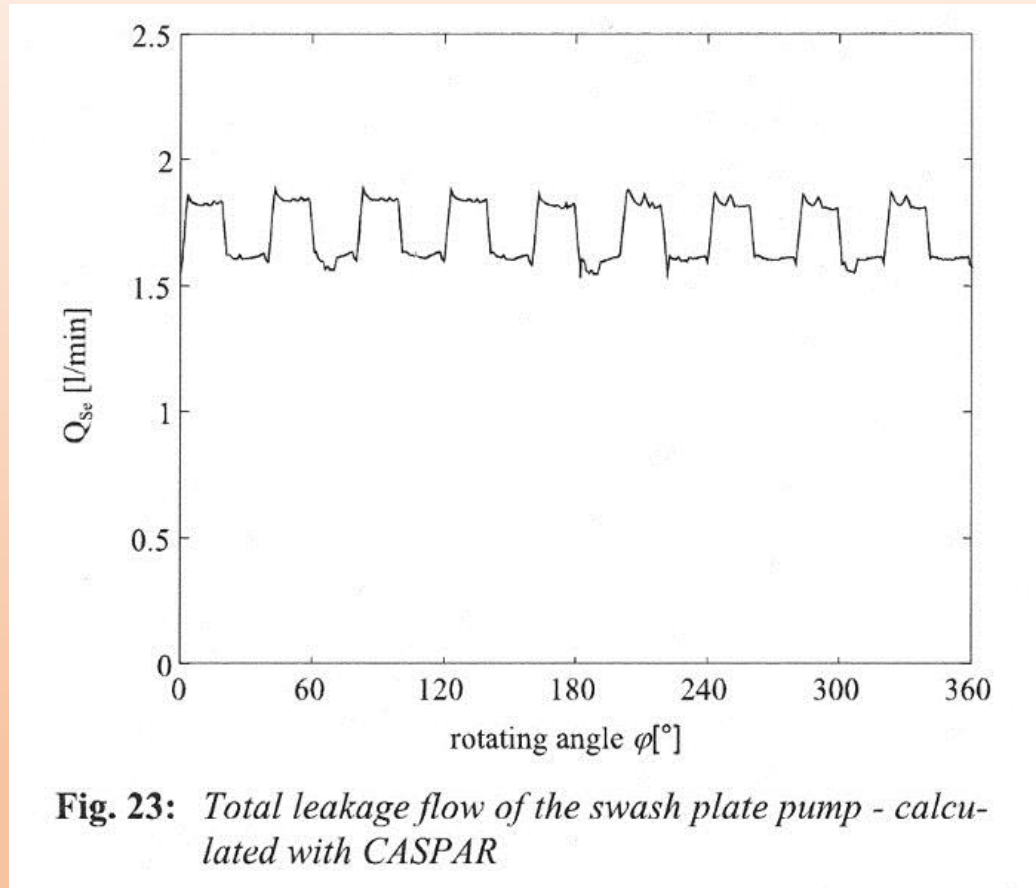
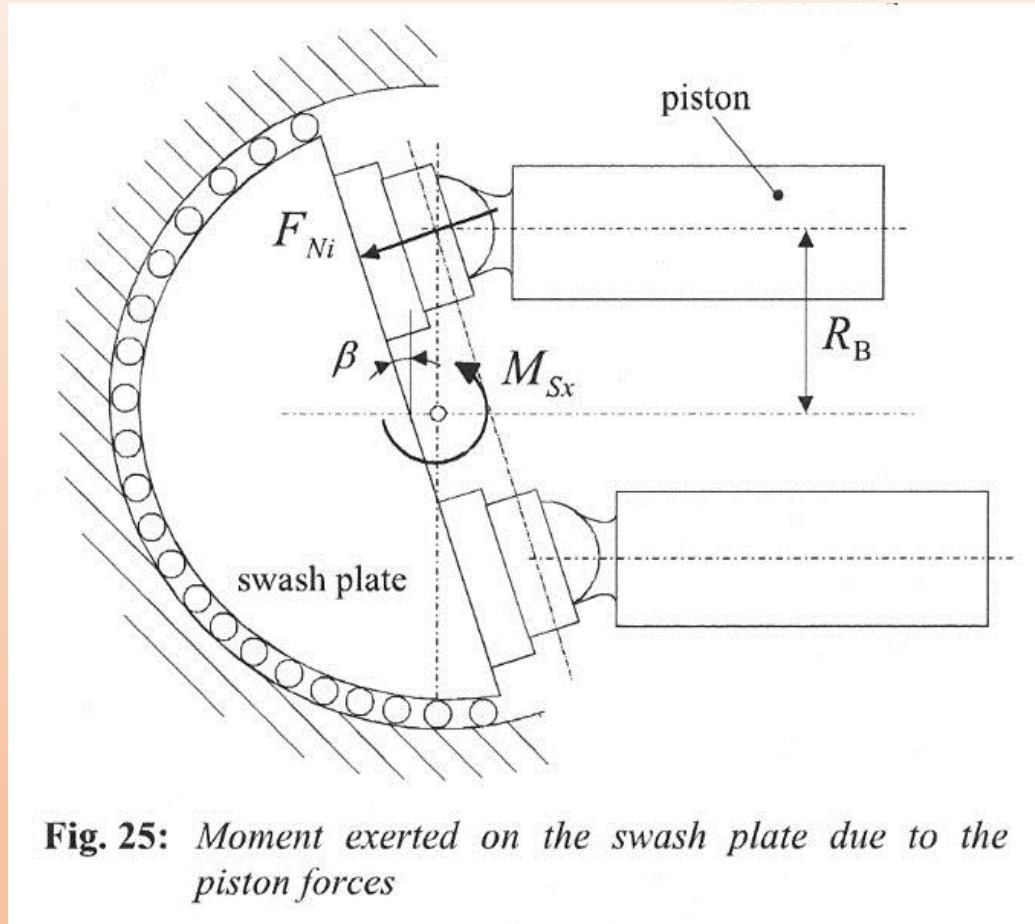


Fig. 23: *Total leakage flow of the swash plate pump - calculated with CASPAR*

Simulation results – total losses ...

- Experimental leakage ~ 1.70 lpm
- Experimental power loss due to friction ~ 10.07 kW
(CASPER: 8.77 kW)

**Simulation results – swash plate moment ...**

- Average moment for the considered operating point is 17.98 Nm



Conclusion ...

- Leakage and viscous friction have been simulated using a sophisticated numerical program
- Elasto-hydrodynamic effects are not included here ...
- A tool for improving the design, to improve the efficiency of the machine
- “A simulation tool cannot replace experiments.”

PHYSICAL LIMITATIONS FOR THE BANDWIDTH FREQUENCY OF AN AXIAL PISTON PUMP

Physical Limitations for the Bandwidth Frequency of a Pressure Controlled, Axial-Piston Pump

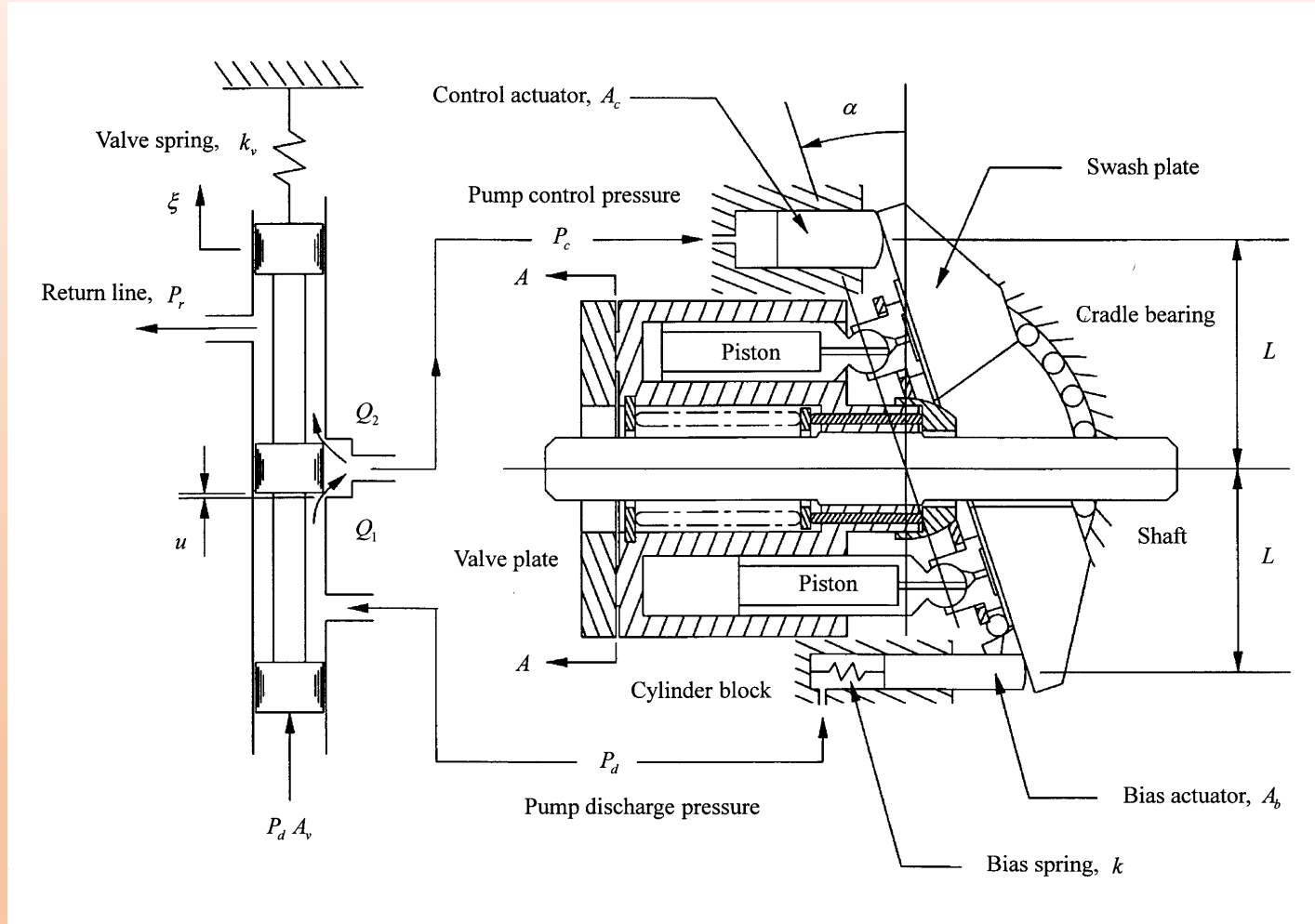
Noah D. Manring and Viral S. Mehta

Journal of Dynamic Systems, Measurement, and Control

November 2011, Vol 133, 061005-1-12

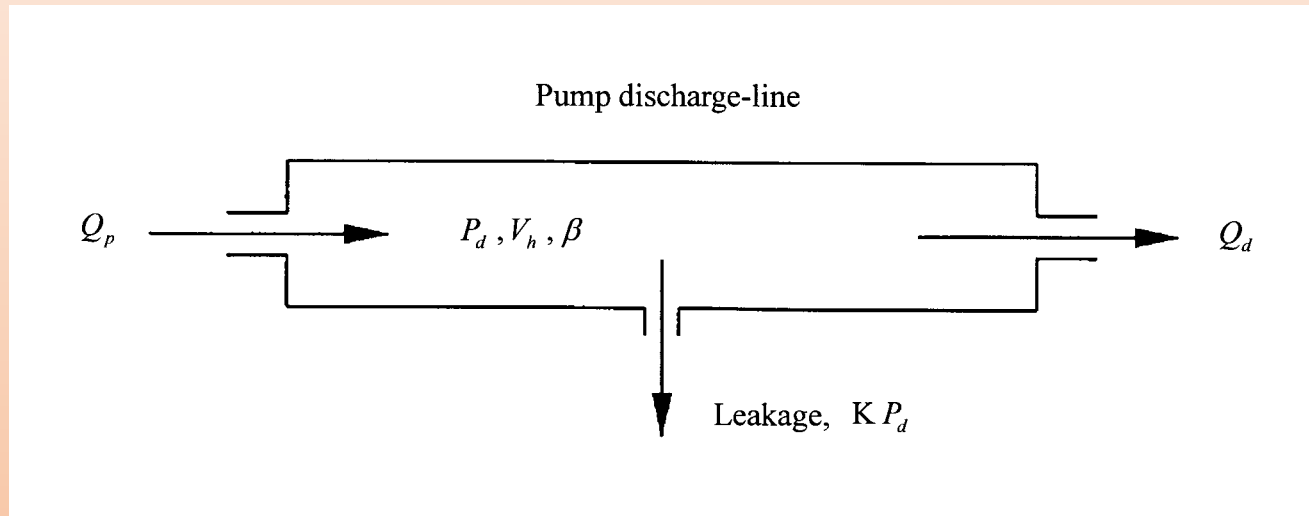
Dedicated to Monika

Pump Description



Analysis

Discharge pressure ...



Pressure rise-rate equation ...

$$\frac{V_h}{\beta} \frac{dP_d}{dt} = Q_p - Q_d - K P_d \quad ,$$

Pump flow ...

$$Q_p = \frac{N A_p r \omega \tan(\alpha)}{\pi} \quad ,$$

$$Q_p = G_p \alpha \quad \text{where} \quad G_p = \frac{N A_p r \omega}{\pi} \quad .$$

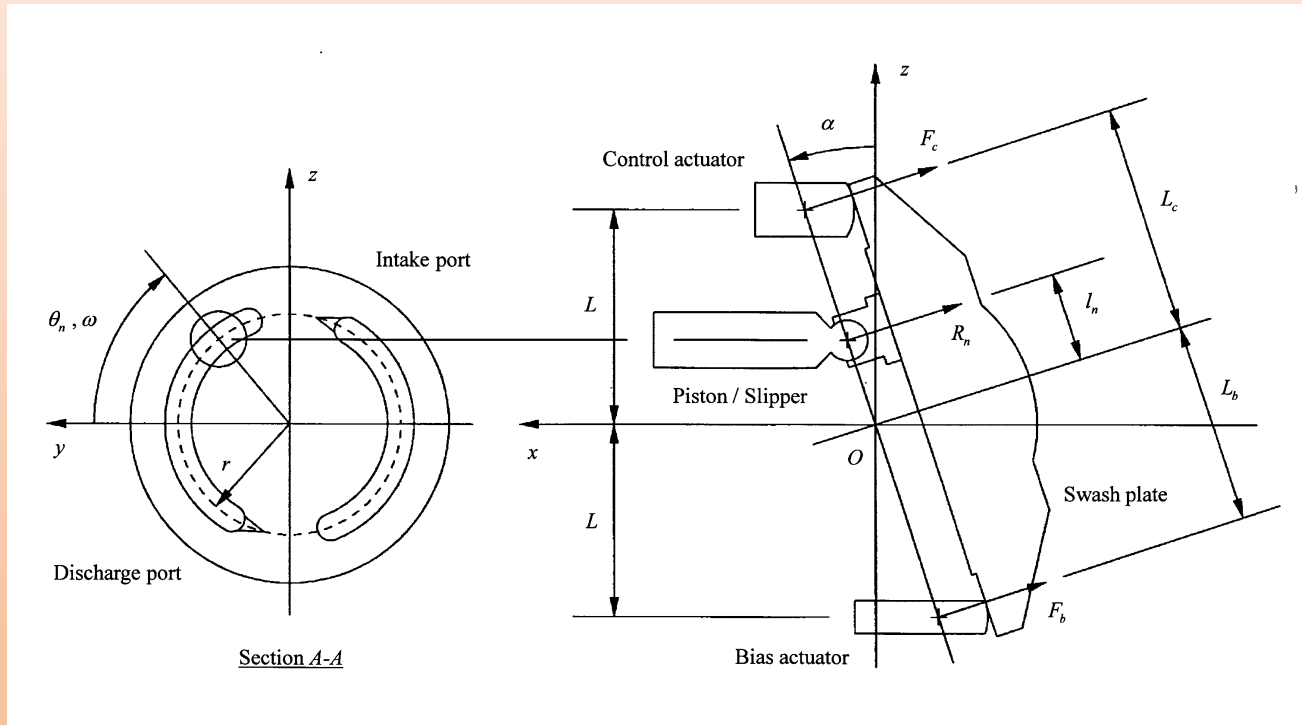
Discharge flow model ...

$$Q_d = Q_{p_o} - K P_{d_o} \quad ,$$

Summary ...

$$\frac{V_h}{\beta} \frac{dP_d}{dt} + K (P_d - P_{d_o}) = G_p (\alpha - \alpha_o) \quad .$$

Swash-plate angle...



Angular momentum ...

$$I \frac{d^2 \alpha}{dt^2} = -C \frac{d\alpha}{dt} + F_b L_b - F_c L_c - \sum_{n=1}^N R_n l_n \quad ,$$

Bias actuator force ...

$$F_b = -M_b L \frac{d^2 \alpha}{dt^2} + P_d A_b + F_o - k L \alpha \quad .$$

Control actuator force ...

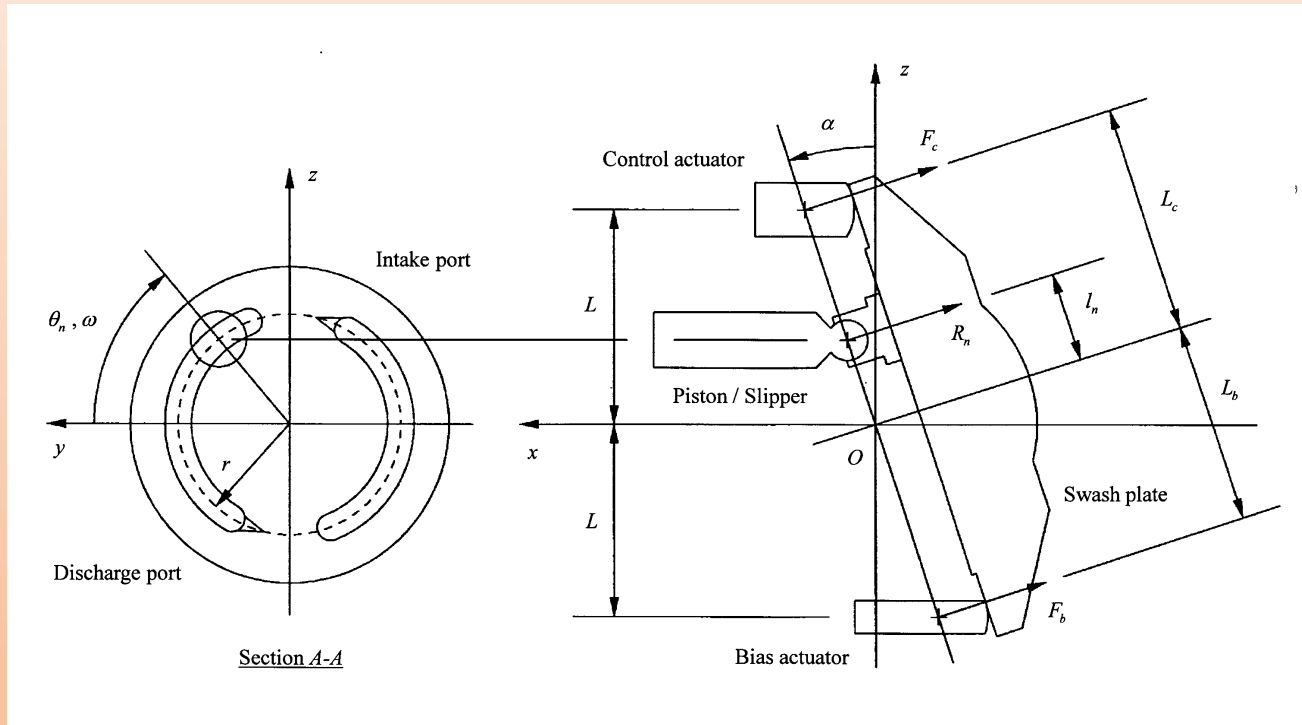
$$F_c = M_c L \frac{d^2 \alpha}{dt^2} + P_c A_c \quad .$$

Slipper reaction ...

$$R_n = M_p r \sin(\theta_n) \frac{d^2 \alpha}{dt^2} + 2M_p r \cos(\theta_n) \omega \frac{d\alpha}{dt} - M_p r \sin(\theta_n) \omega^2 \alpha + P_n A_p \quad ,$$

Continued on the next slide ...

Swash-plate angle...



Equation of motion ...

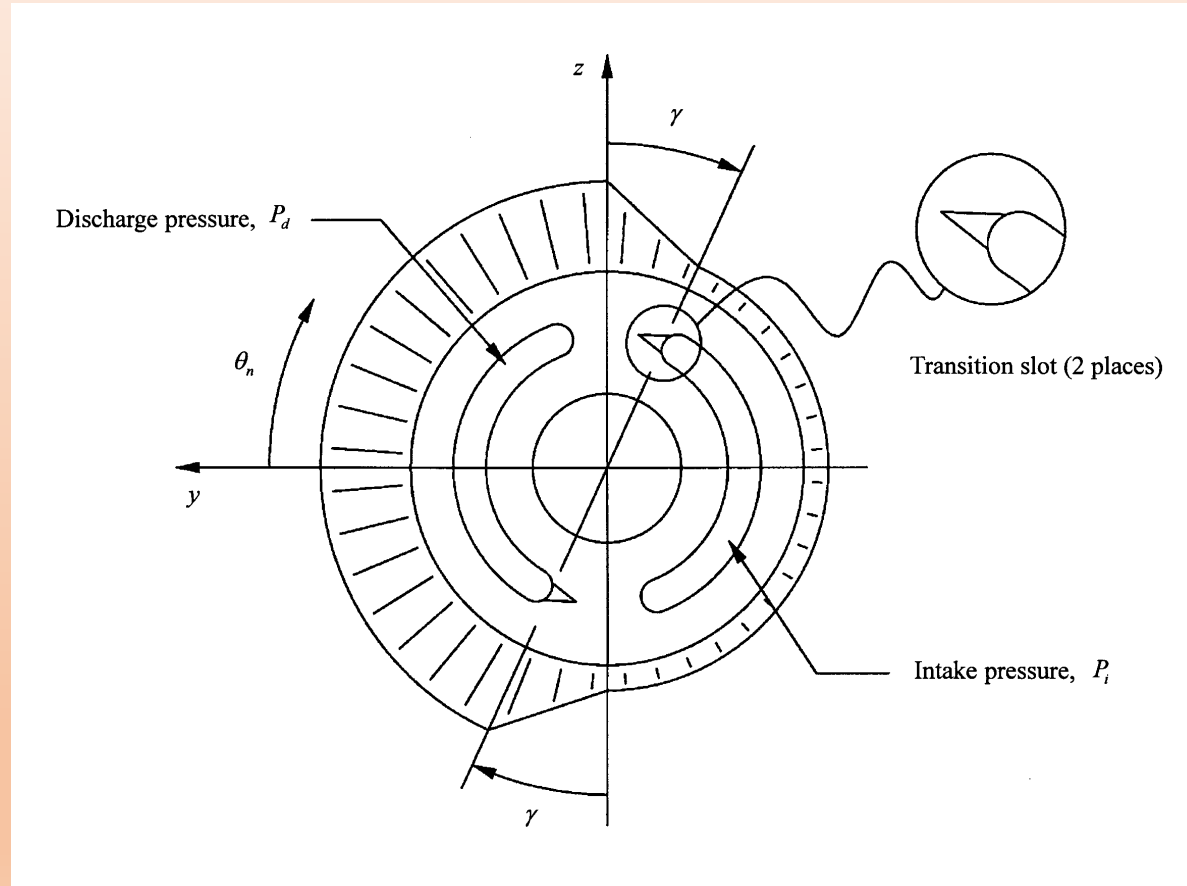
$$\left(I + [M_b + M_c]L^2 + \frac{N}{2}M_p r^2 \right) \frac{d^2\alpha}{dt^2} + C \frac{d\alpha}{dt} + \left(kL^2 - \frac{N}{2}M_p r^2 \omega^2 \right) \alpha = (P_d A_b - P_c A_c)L + F_o L - A_p r \sum_{n=1}^N P_n \sin(\theta_n) \quad ,$$

where the following identities have been used ...

$$\sum_{n=1}^N \sin^2(\theta_n) = \frac{N}{2} \quad \text{and} \quad \sum_{n=1}^N \sin(\theta_n) \cos(\theta_n) = 0 \quad .$$

Piston pressure terms must be studied ...

(Piston pressure ...)



Discontinuous approximation ...

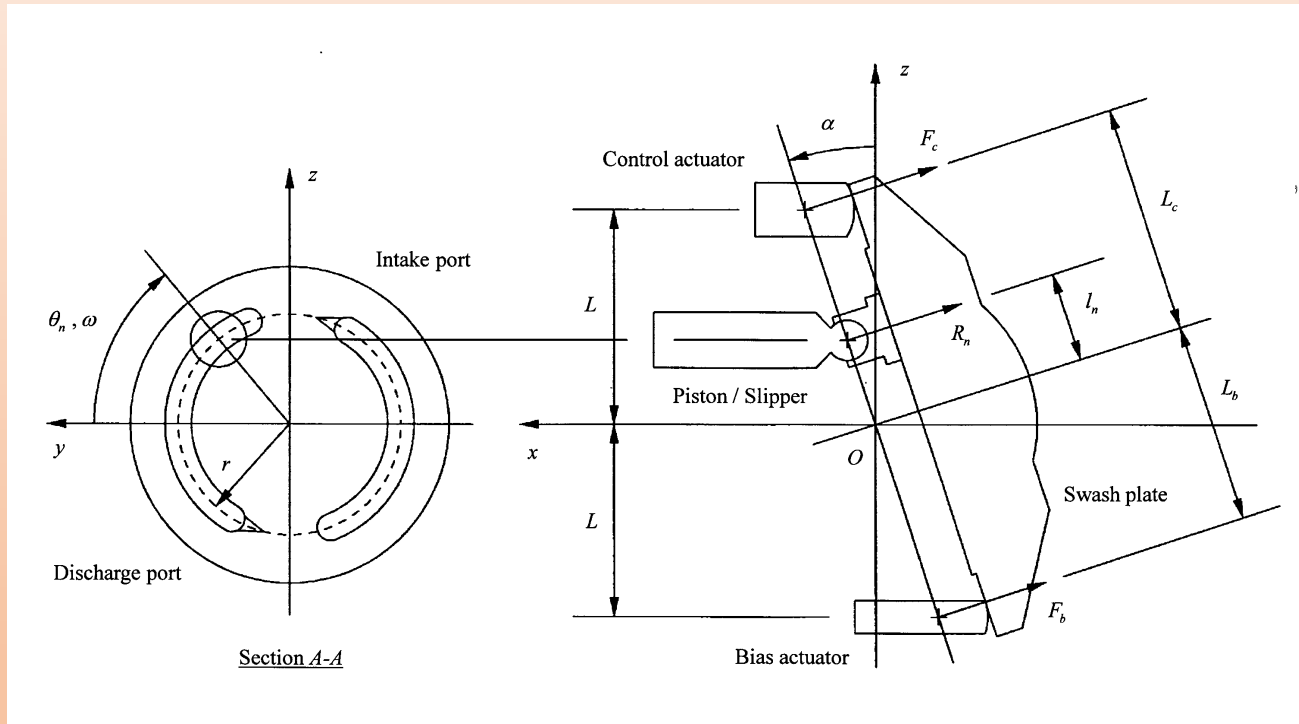
$$P_n = \begin{cases} P_d & -\frac{\pi}{2} + \gamma < \theta_n < \frac{\pi}{2} \\ P_d - \frac{(P_d - P_i)}{\gamma} (\theta_n - \pi/2) & \frac{\pi}{2} < \theta_n < \frac{\pi}{2} + \gamma \\ P_i & \frac{\pi}{2} + \gamma < \theta_n < \frac{3\pi}{2} \\ P_i + \frac{(P_d - P_i)}{\gamma} (\theta_n - 3\pi/2) & \frac{3\pi}{2} < \theta_n < \frac{3\pi}{2} + \gamma \end{cases}$$

Integral average ...

$$\sum_{n=1}^N P_n \sin(\theta_n) \rightarrow \frac{N}{2\pi} \int_0^{2\pi} P_n \sin(\theta_n) d\theta_n = \frac{N}{2\pi} (P_d - P_i) \gamma \quad ,$$

Substitution ...

Swash-plate angle...



Equation of motion ...

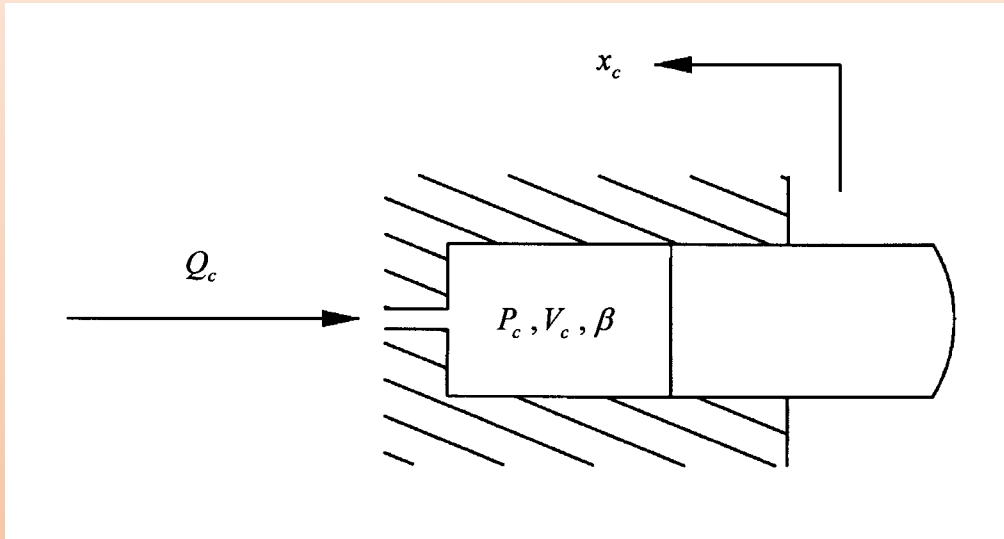
$$\left(I + [M_b + M_c] L^2 + \frac{N}{2} M_p r^2 \right) \frac{d^2 \alpha}{dt^2} + C \frac{d\alpha}{dt} + \left(k L^2 - \frac{N}{2} M_p r^2 \omega^2 \right) (\alpha - \alpha_o) = \left(A_b L - \frac{N A_p r \gamma}{2\pi} \right) (P_d - P_{d_o}) - A_c L (P_c - P_{d_o} / 2) ,$$

where the steady-state moment for the preload of the bias spring was substituted into the equation ...

$$F_o L = \left(k L^2 - \frac{N}{2} M_p r^2 \omega^2 \right) \alpha_o + \frac{N A_p r \gamma}{2\pi} (P_{d_o} - P_i) - \left(A_b - \frac{A_c}{2} \right) L P_{d_o} ,$$

Pressure in the control actuator must be studied ...

Control pressure ...

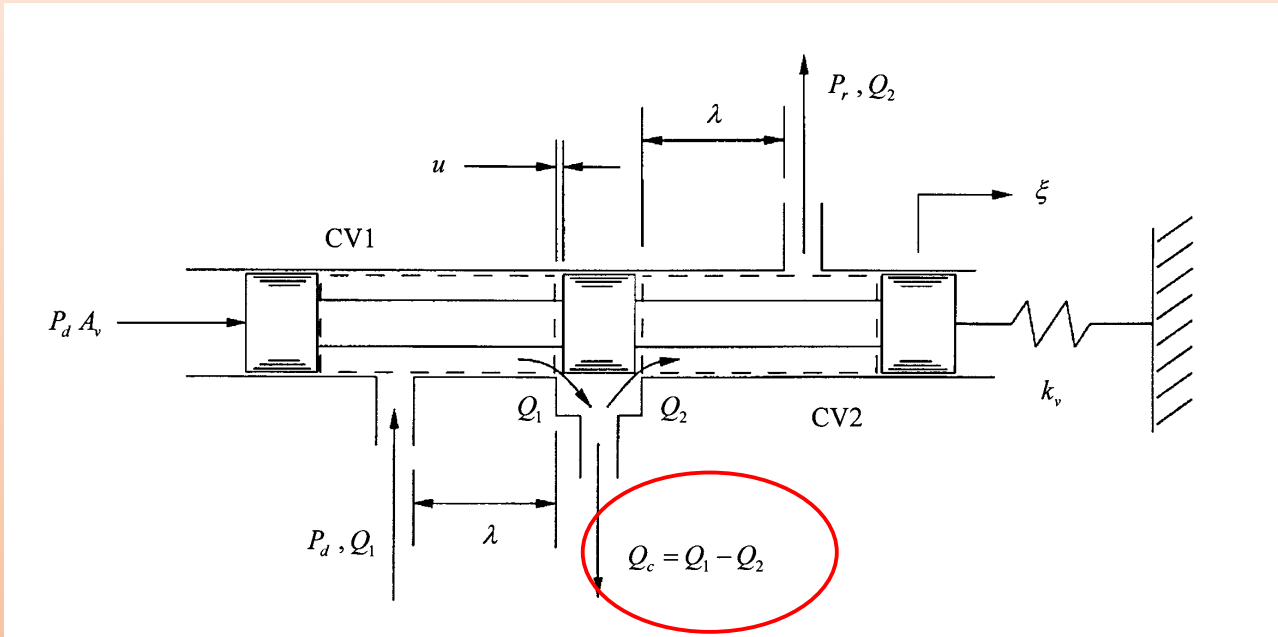


Pressure rise-rate equation ...

$$\frac{V_c}{\beta} \frac{dP_c}{dt} = Q_c + A_c L \frac{d\alpha}{dt} .$$

Control flow to the actuator must be studied ...

(Control flow ...)



Control flow ...

$$Q_c = Q_1 - Q_2 \quad .$$

Metering land flow ...

$$Q_1 = A_1 C_d \sqrt{\frac{2}{\rho} (P_d - P_c)} \quad \text{and} \quad Q_2 = A_2 C_d \sqrt{\frac{2}{\rho} (P_c - P_r)} \quad ,$$

Linearized results ...

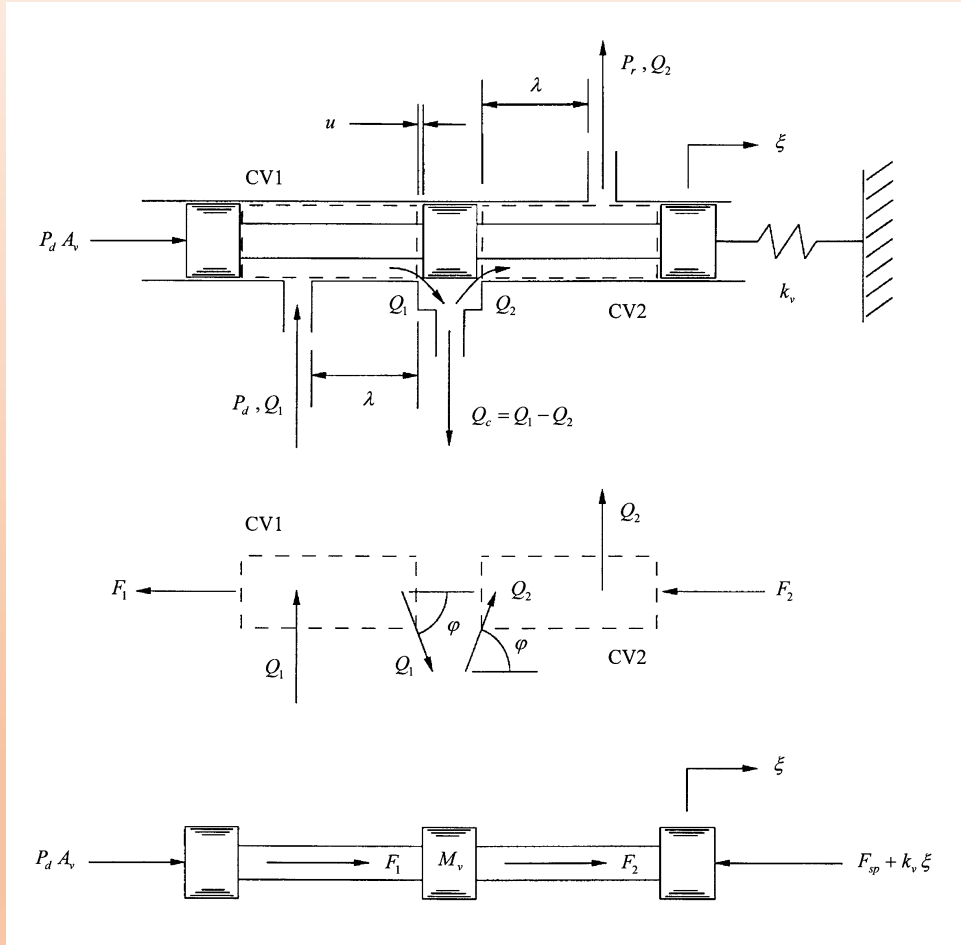
$$Q_c = 2 K_q \xi + K_c (P_d - 2P_c) \quad .$$

Where the valve coefficients are given by

$$K_q = C_d \sqrt{\frac{P_{d_o}}{\rho}} \left. \frac{\partial A_{1,2}}{\partial \xi} \right|_o \quad \text{and} \quad K_c = \frac{C_d A_o}{\sqrt{\rho P_{d_o}}} \quad ,$$

We need an equation of motion for the valve ...

Equation of motion ...



Equation of motion ...

$$M_v \frac{d^2 \xi}{dt^2} = P_d A_v - F_{sp} - k_v \xi + F_1 + F_2 \quad ,$$

Reynolds transport theorem ...

$$F_1 + F_2 = -\rho \lambda K_c \frac{dP_d}{dt} - K_{fc} (P_d - 2P_c) - 2K_{fq} \xi \quad ,$$

Where the flow force coefficients are ...

$$K_{fq} = P_{d_o} C_d^2 \cos(\varphi) \left| \frac{\partial A_{1,2}}{\partial \xi} \right|_o \quad \text{and} \quad K_{fc} = 2 A_o C_d^2 \cos(\varphi) \quad .$$

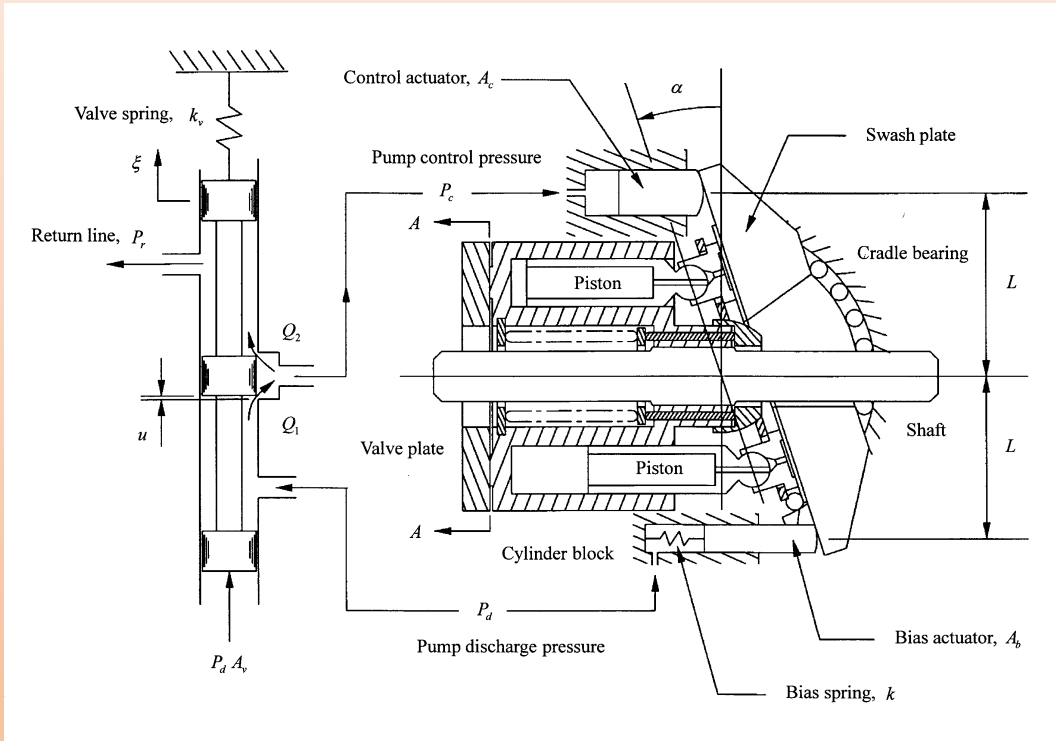
Summary ...

$$M_v \frac{d^2 \xi}{dt^2} + (k_v + 2K_{fq}) \xi = (P_d - P_{d_o}) A_v - K_{fc} (P_d - 2P_c) - \rho \lambda K_c \frac{dP_d}{dt} \quad ,$$

Putting everything together ...

Summary

Nondimensional model ...



discharge pressure: $\frac{d\hat{P}_d}{dt} + \Psi_1(\hat{P}_d - 1) = (\hat{\alpha} - 1)$,

swash-plate motion: $\Psi_2 \frac{d^2 \hat{\alpha}}{dt^2} + \Psi_3 \frac{d\hat{\alpha}}{dt} + \Psi_4(\hat{\alpha} - 1) = \Psi_5(\hat{P}_d - 1) - (\hat{P}_c - 1)$,

control pressure: $\Psi_6 \frac{d\hat{P}_c}{dt} = \hat{\xi} + \Psi_7(\hat{P}_d - 1) - \Psi_7(\hat{P}_c - 1) + \Psi_8 \frac{d\hat{\alpha}}{dt}$, and

spool-valve motion: $\Psi_9 \frac{d^2 \hat{\xi}}{dt^2} + \Psi_{10} \hat{\xi} = (1 - \Psi_{11})(\hat{P}_d - 1) + \Psi_{11}(\hat{P}_c - 1) - \Psi_{12} \frac{d\hat{P}_d}{dt}$,

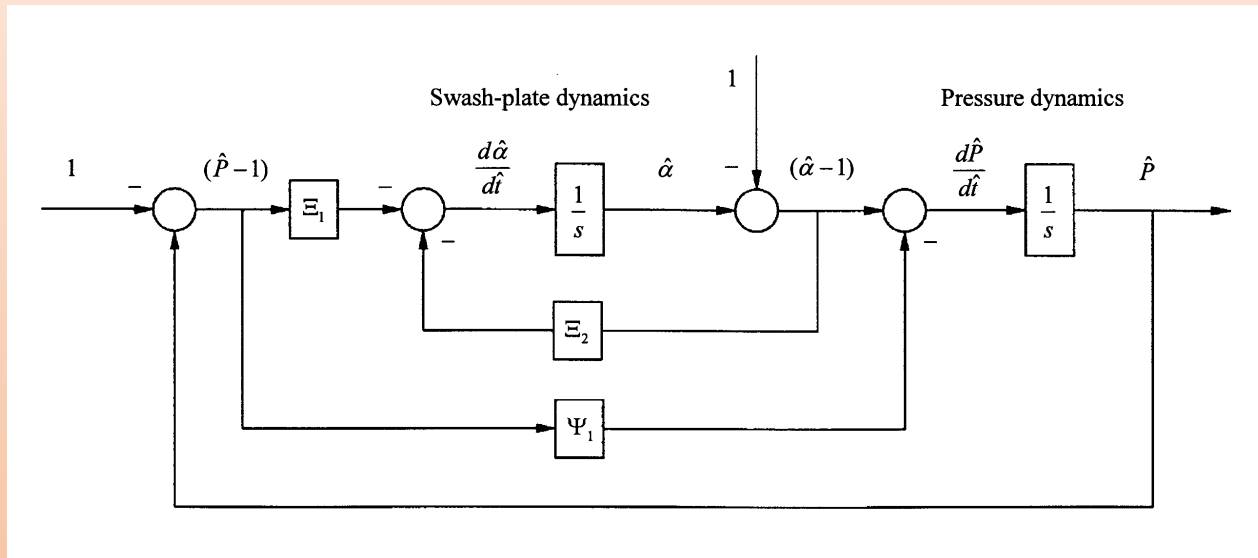
$$\Psi_1 = \frac{K P_{d_o}}{G_p \alpha_o} , \quad \Psi_2 = \frac{2 \left(I + [M_b + M_c] L^2 + \frac{N}{2} M_p r^2 \right) \alpha_o}{A_c L P_{d_o} \tau^2} , \quad \Psi_3 = \frac{2 C \alpha_o}{A_c L P_{d_o} \tau} ,$$

$$\Psi_4 = \frac{2 \left(k L^2 - \frac{N}{2} M_p r^2 \omega^2 \right) \alpha_o}{A_c L P_{d_o}} , \quad \Psi_5 = 2 \left(\frac{A_b}{A_c} - \frac{N A_p r \gamma}{2 \pi A_c L} \right) , \quad \Psi_6 = \frac{V_c P_{d_o}}{4 \beta K_q u \tau} ,$$

$$\Psi_7 = \frac{K_c P_{d_o}}{2 K_q u} , \quad \Psi_8 = \frac{A_c L \alpha_o}{2 K_q u \tau} , \quad \Psi_9 = \frac{M_v u}{A_v P_{d_o} \tau^2} , \quad \Psi_{10} = \frac{(k_v + 2K_{f_q}) u}{A_v P_{d_o}} ,$$

$$\Psi_{11} = \frac{K_{f_c}}{A_v} , \quad \text{and} \quad \Psi_{12} = \frac{\rho \lambda K_c}{A_v \tau} .$$

Reduced order model ...



Second order system ...

$$\begin{Bmatrix} \frac{d\hat{P}}{dt} \\ \frac{d\hat{\alpha}}{dt} \end{Bmatrix}^T = \begin{bmatrix} -\Psi_1 & 1 \\ -\Xi_1 & -\Xi_2 \end{bmatrix} \begin{Bmatrix} (\hat{P}-1) \\ (\hat{\alpha}-1) \end{Bmatrix},$$

where ...

$$\Xi_1 = \frac{1 + (1 - \Psi_5)(\Psi_7\Psi_{10} - \Psi_{11})}{\Psi_8\Psi_{10}} \quad \text{and} \quad \Xi_2 = \frac{\Psi_4(\Psi_7\Psi_{10} - \Psi_{11})}{\Psi_8\Psi_{10}}.$$

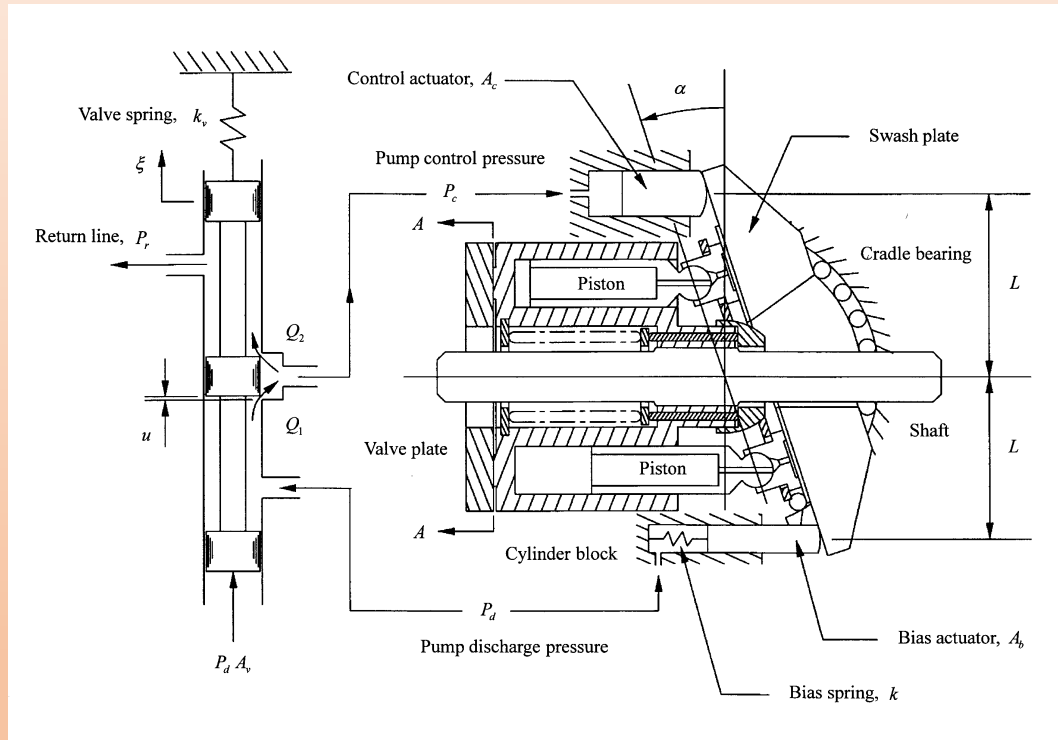
Closed form bandwidth frequency ...

$$\hat{\omega}_{bw} = \hat{\omega}_n \left\{ 1 - 2\zeta^2 + \sqrt{2 - 2\zeta^2(1 - \zeta^2)} \right\}^{\frac{1}{2}}.$$

where ...

$$\hat{\omega}_n = \sqrt{\Psi_1\Xi_2 + \Xi_1} \quad \text{and} \quad \zeta = \frac{\Psi_1 + \Xi_2}{2\hat{\omega}_n}.$$

Perturbations ...



Closed form bandwidth frequency ...

$$\hat{\omega}_{bw} = \hat{\omega}_n \left\{ 1 - 2\zeta^2 + \sqrt{2 - 2\zeta^2(1 - \zeta^2)} \right\}^{\frac{1}{2}}$$

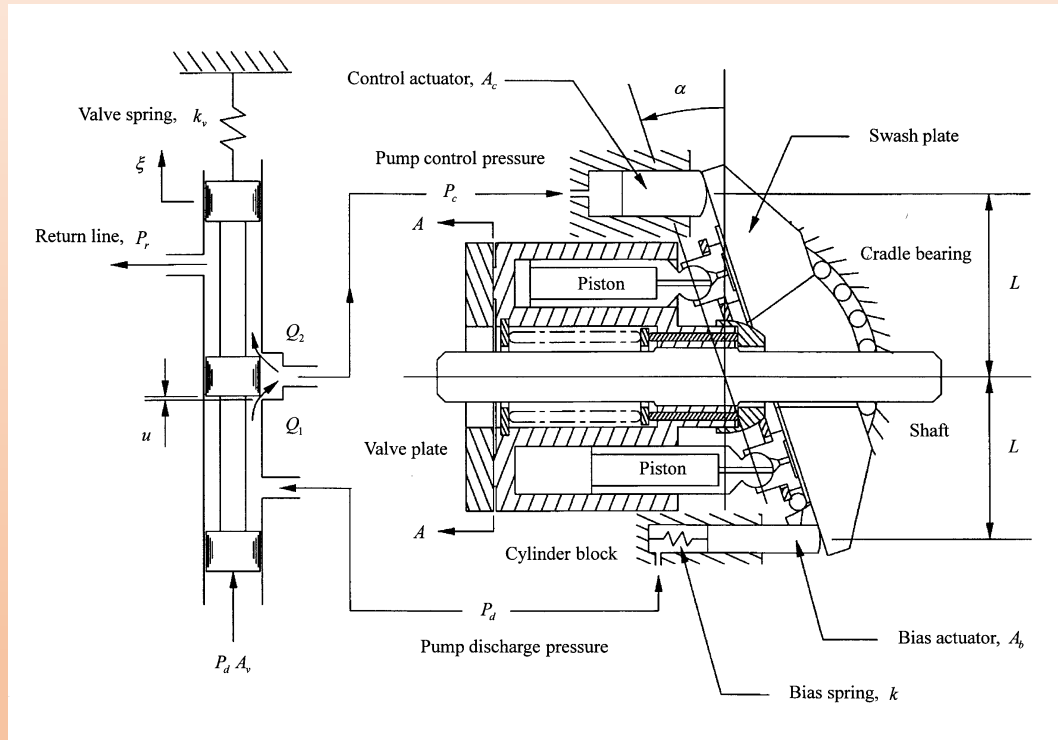
where ...

$$\hat{\omega}_n = \sqrt{\Psi_1 \Xi_2 + \Xi_1} \quad \text{and} \quad \zeta = \frac{\Psi_1 + \Xi_2}{2 \hat{\omega}_n}$$

Nondimensional sensitivity coefficients ...

$$\hat{\omega}_{bw} = \hat{\omega}_{bw_o} + \frac{\partial \hat{\omega}_{bw}}{\partial \Psi_1} \Big|_o (\Psi_1 - \Psi_{1_o}) + \frac{\partial \hat{\omega}_{bw}}{\partial \Psi_4} \Big|_o (\Psi_4 - \Psi_{4_o}) + \dots + \frac{\partial \hat{\omega}_{bw}}{\partial \Psi_{11}} \Big|_o (\Psi_{11} - \Psi_{11_o})$$

Perturbations ...



Results ...

Table 2 Bandwidth-frequency sensitivity coefficients

Coefficient	Physical description	Numerical value
$\frac{\partial \dot{\omega}_{bc}}{\partial \Psi_{1o}}$	Pump leakage	-0.114
$\frac{\partial \dot{\omega}_{bc}}{\partial \Psi_{4o}}$	Swash-plate spring rate	-2.82
$\frac{\partial \dot{\omega}_{bc}}{\partial \Psi_{5o}}$	Discharge pressure moment exerted on the swash plate	-1.67
$\frac{\partial \dot{\omega}_{bc}}{\partial \Psi_{7o}}$	Open-centered valve flow into the control actuator	0.735
$\frac{\partial \dot{\omega}_{bc}}{\partial \Psi_{8o}}$	Volumetric change of the control actuator	-389
$\frac{\partial \dot{\omega}_{bc}}{\partial \Psi_{10o}}$	Spool valve spring rate	-9.51
$\frac{\partial \dot{\omega}_{bc}}{\partial \Psi_{11o}}$	Pressure induced flow-force on the spool valve	-1.06

Closed form bandwidth frequency ...

$$\Psi_8 = \frac{A_c L \alpha_o}{2K_q u \tau}$$

Conclusions

- 1. The pressure controlled pump is a second-order, underdamped system which exhibits overshoot and oscillation before reaching steady-state. Dominant transients are the discharge pressure and the swash-plate angle.**
- 2. By far, the most effective way to increase the bandwidth frequency of the pump is to REDUCE the swept volume of the actuator, and to INCREASE the flow gain of the valve.**

CONCLUDING REMARKS



1955 - 2018

- 1. She was a bright light in the fluid power community for over 30 years (vibrant, joyful, excited).**
- 2. She contributed significantly to the art and science of designing axial piston pumps and motors.**
- 3. She was a friend to all of us.**
- 4. She will be missed.**